Article

Contribution of Reverse Dune Migration to Stabilization of a Transgressive Coastal Dune Field at Lagoa do Peixe National Park Dune Field (South of Brazil)

Rogério Portantiolo Manzolli [1],*, Luana Carla Portz [1], Angela Fontán-Bouzas [2,3], Volney Junior Borges Bitencourt [4] and Javier Alcántara-Carrió [1]

[1] Department of Geology and Geochemistry, Universidad Autónoma de Madrid, 28049 Madrid, Spain; luana.portz@uam.es (L.C.P.); javier.alcantara@uam.es (J.A.-C.)

[2] Department of Geodynamics, Stratigraphy and Paleontology, Faculty of Geological Sciences, Complutense University of Madrid, C/José Antonio Novais, 12, 28040 Madrid, Spain; anfontan@ucm.es

[3] CIM-UVIGO GEOMA, University of Vigo, 36310 Vigo, Spain

[4] Instituto do Meio Ambiente de Santa Catarina (IMA), Florianópolis 88020-300, Brazil; volneybitencourt@ima.sc.gov.br

* Correspondence: rogerio.manzolli@uam.es

Abstract: Coastal dunes that transgress typically move landward, while their reverse movement is not well understood. The article discusses the study of barchan and barchanoid dunes in the Lagoa do Peixe National Park in the coastal plain of Rio Grande do Sul, Brazil. The aim of the study is to analyze seasonal patterns and long-term trends in the direction and migration rates of these dunes, which can pose a threat to the lagoon if they invade its space. The crest migration of 12 dunes was monitored by satellite images between July 2003 and December 2018, and DGPS topographic surveys were performed on five dunes between 2010 and 2018. The migration rates obtained were combined with an analysis of the meteorological data and calculations of the drift potential for eolian sediment transport. The wind regime in the study area shows a multidirectional pattern, with the predominant wind direction being from the NE, followed by the ENE direction. The wind direction also exhibits a seasonal behavior, with the winds from the first quadrant being dominant during spring and summer months and a gradual increase in winds from the second and third quadrants from the end of summer to winter. The dune crest migration rates in the Lagoa do Peixe National Park show an average of 16.55 m·yr^{-1} towards WSW–W, mainly controlled by the direction of the effective winds. However, intense SSW–WSW winds caused by cold fronts in the past generate the reverse migration of dunes towards ENE–E. The reverse migration of dunes explains the steadiness of the dune fields at CPRGS and is a factor controlling dune stabilization and the geomorphological evolution of transgressive coastal dune fields. The article highlights the importance of monitoring dune movement to understand their responses to natural and anthropogenic stressors and to protect sensitive ecosystems.

Keywords: coastal dune; barchan dune; sediment transport; drift potential; migration rate

1. Introduction

Coastal dunes are naturally developed on sandy beaches, from tropical to arctic conditions [1,2]. They constitute large sediment accumulations of which form, size, and orientation vary according to the beach profile, coast orientation, direction and speed of the wind, particle size, and type of vegetation of each location [3–5].

Coastal dunes are dynamic environments that develop and evolve as the result of a complex interaction between sand, wind, vegetation, and external pressures [6]. They form when sediment deposited over the beach dries, and then it is blown by the wind landward [7]. Their occurrence is, therefore, directly related to sand supply and favorable

wind patterns [8]. Coastal dunes tend to develop in beaches where there is a large sediment supply, enough wind to move this sediment landward, and a backshore space to accumulate this sediment [9]. The sediment availability depends on both the volume of sediments and its grain size [10,11]. The beach profile also controls the development of dunes; usually, the development of dunes is favored in dissipative beaches better than in reflective ones [6].

The geomorphological evolution and stabilization of coastal dune fields can be primarily related to either climate variations or human interferences, which are able to transform active dunes into stable ones and vice-versa. Changes in vegetation cover, due to both climate variations and human activities, contribute to dune stabilization [12–14]. The model developed by [15] predicts that long droughts with strong winds might result in the reactivation of dunes. Even relatively small changes in climatological parameters can generate changes in both vegetal cover and geomorphological configurations [15–17]. Monitoring the dune movement is essential in this scenario; dune migration rates can provide essential information about the dunes' responses to natural (wind and rain regimes, vegetation cover) and anthropogenic stressors [18].

The monitoring of dune systems is being conducted in several regions, using different techniques after the spatial and temporal scales of the study, such as drones. Thus, aerial photographs and/or satellite images are often used to evaluate changes in the dunes' position and morphology, particularly for long-term studies, i.e., ten years or more [18–26] By contrast, short-term studies and fieldwork measurements with GPS were initially the most usual method for mapping and measurements of the dunes' slip faces [27–29]. However, nowadays, LiDAR and drone systems are more frequently used [30–33].

Most of the dune fields in the coastal plain of Rio Grande do Sul (CPRGS) are currently located in the Middle and South regions. These dune fields have a history of stabilization and vegetation growth, which are related to high precipitation levels, reduced wind speed, and large sediment supply [34], as well as alterations in the regional hydrology that influence groundwater levels [35]. The objective of this study is to analyze the normal and reverse migration of the transgressive dunes, related to the typical annual wind patterns and the occurrence of cold fronts, respectively, and their implications for the stabilization of the dune field of the Lago do Peixe Natural Park.

2. Study Area

The study area is located on the dune field close to the Peixe lagoon (middle region of the CPRGS). This dune field and coastal lagoon form the Lagoa do Peixe National Park, designated as a Ramsar site, but the lagoon is at risk of being invaded by the transgressive barchan and barchanoid dunes.

2.1. Regional Setting and Study Area—Relevance of Dune Fields in Rio Grande do Sul

The relief adjacent to the coast of Rio Grande do Sul varies abruptly. The North region is formed by the high mountains of the Serra Geral escarpment; in the South, the escarpment ends, and a large alluvial coastal plain prevails with a flat and open surface. The CPRGS was reworked during the transgressive and regressive cycles of the Quaternary. Initially, deposits of coalescing alluvial fans developed at the end of the Tertiary because of the transport processes of terrigenous clastic sediments associated with upland environments. Afterwards, these deposits were laterally overlapped by four barrier-lagoon depositional systems, whose formation was controlled by the sea level fluctuations during the Quaternary (Barriers I, II, and III, from the Pleistocene, and Barrier IV, from the Holocene), creating a succession of marine and lagoon terraces [36–38]. Consequently, this alluvial plain has a complex system of sandy barriers that protect a large lagoon system (Patos lagoon and Mirim lake) and a series of other waterbodies, isolated or interconnected with the sea through narrow and shallow channels [36].

The coast of Rio Grande do Sul has several factors that favors the formation and evolution of one of the most extensive systems of the coastal dunes of Brazil, with low roughness topography (coastal plain), appropriate wind regimes, and a large supply of fine

quartz sand [39]. In these sectors, transgressive dune fields are formed. These are broad, eolian sand deposits formed by the downwind movement of sand sheets and free dunes over vegetated to semi-vegetated terrain [40]. They range from small sheets to large-scale sand seas, typically bordered by precipitation ridges and often fronted by deflation basins and plains [41]. Barchan dunes and barchanoid ridges are common features along the southern Brazilian coastal dunes [34,42–44]. In some sectors with larger dune fields (such as the middle of RS), transverse dunes can also be identified. In the marginal portions of the dune fields, places with less sand and a more abundant presence of vegetation, there are predominant parabolic sand dunes [45]. In fact, in Rio Grande do Sul, the dunes are located along the entire coast, being drastically reduced in sectors where urbanization is more developed [46]; in such cases, only frontal dunes are formed [45,47–50].

The Lagoa do Peixe National Park (LPNP) is in the Middle region of the CPRGS, between the Patos lagoon and the Atlantic Ocean (Figure 1). The Park includes several ecosystems that are representative of the region, such as beaches, dunes, salt marshes, saline swamps, and the lagoon.

The Peixe lagoon is 35 km long, 1 m wide, and approximately 30 cm deep. The origin of the Peixe lagoon is related to the formation of a marine and eolian sediment barrier during the Holocene transgression. In fact, it corresponds to the lagoon portion of the Barrier-Lagoon System IV. Moreover, there is a direct connection with the sea in the southern sector of the lagoon; it happens through an artificial opening of the barrier during winter months that persists until the beginning of summer, when the prevailing winds deposit marine sediments, blocking the opening [51].

The dunes cover approximately 45% of the LPNP area [52], forming a continuous band alongshore. They are mainly composed of unconsolidated quartz sand with grain size (mean sediment grain size 0.215 mm) [53]. The dunes are very prominent, and they are better represented at the northern area, where the higher dunes with heights over 15 m and perpendicularly orientated in relation to the NE wind direction are located [51]. The width of the dune field varies alongshore of the national park, reaching a maximum of 5.15 km in the north and a minimum of 0.70 km in the south. The speed and direction of dune migration on the east side of the LPNP are currently among the discussion topics regarding management practices. Given the low depth of the lagoon, changes in these patterns could greatly affect the input of sediment to the lagoon system, causing high-impact environmental changes.

2.2. Climate Control of Dune Fields in Rio Grande do Sul

The regional winds blowing in the study area are connected to the atmospheric flow over Rio Grande do Sul. This flow is generated by the interaction among the Atlantic Subtropical Anticyclone, the intermittent movements of polar masses, and the barometric depression of northeastern Argentina [54]. The variations on this atmospheric system result in wind seasonal patterns. During spring and summer, the weather in the coastal plain is usually warm and windy, particularly with winds from NE and E; during fall–winter, the area is dominated by cold fronts coming from SW–NE, oftentimes regularly [55]. The winds intensity varies along the coast, with a positive speed gradient from North to South. In response to the prevailing winds, the free dunes migrate towards SW [29,47,54,56].

The dimensions of the coastal dune fields in CPRGS are associated with wind patterns but also with the rainfall regime of each sector. The dune fields at the northern littoral are narrower (1300 to 1400 m wide) due to the local higher precipitation, lower wind drift potential (DP), and smaller sand supply. Southwards, the dune fields increase their width (reaching 6900 m) as the precipitation decreases, and the wind DP and the sand supply increases in the area [34].
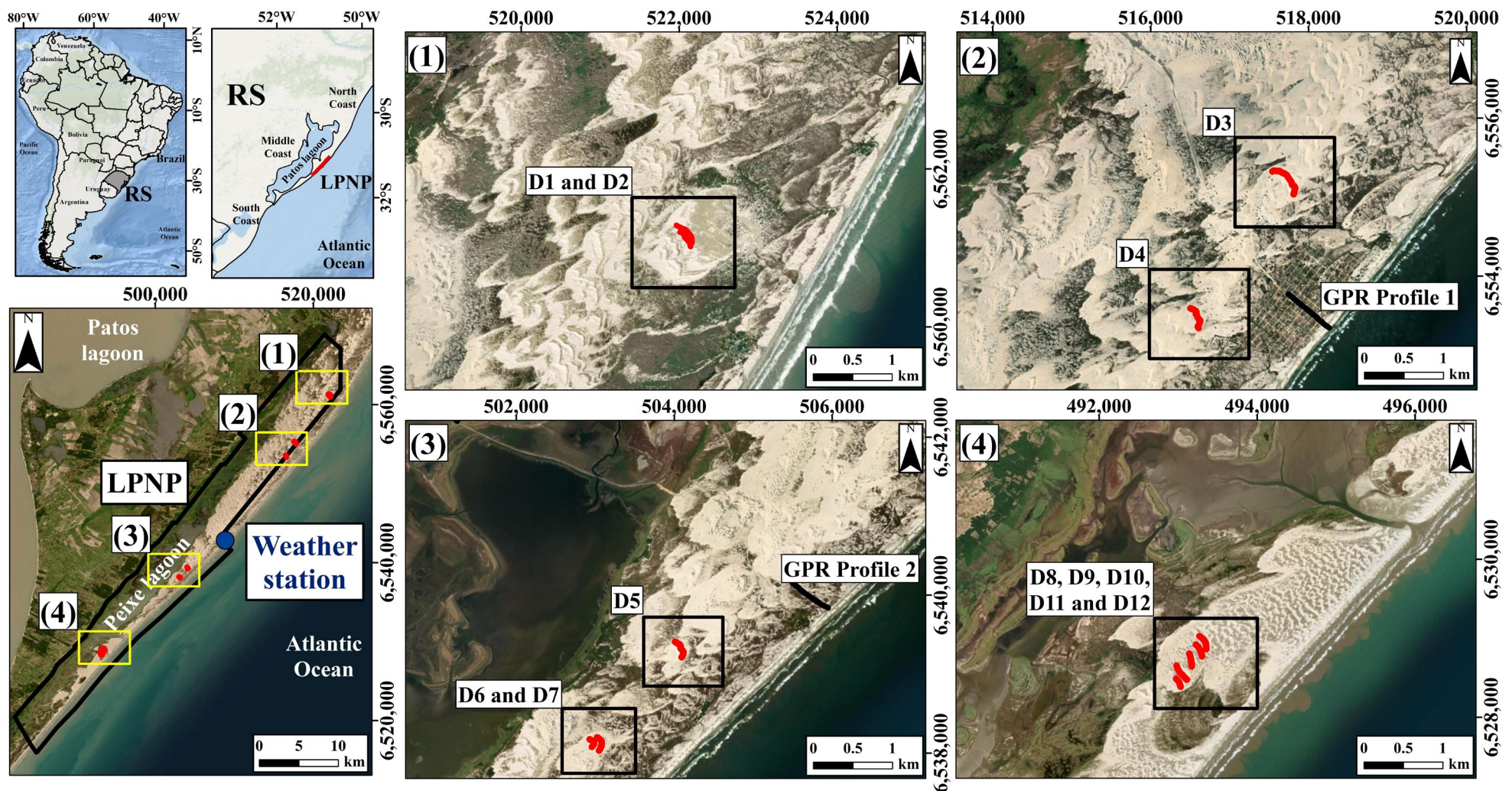
Figure 1. Location of the study area on the middle sector of the coastal plain of Rio Grande do Sul (South of Brazil). On the left image, the black line is delimiting the Lagoa do Peixe National Park, and the blue point is the location of the weather station. In the right images, for sectors 1 to 4, the red lines indicate the crests of the monitored dunes (Image base: ArcMap® 10.8).

2.3. Coastal Barrier Stratigraphy

According to several studies, the stratigraphy of the study area shows thick eolian deposits [57,58]. The GPR surveys conducted at the Peixe lagoon exhibited up to 15 m of thickness [59,60]. This is a result of both the coastline orientation relative to the NE winds [61] and the high sediment supply rate resulting from a jam in the longshore transport [62]. The silting of back-barrier lagoons by the transgression of dune sands provides a platform for barrier translation during the post-glacial marine transgression (PMT). Probably, such processes were operating since before the sea level maximum of the mid-Holocene (~6 ka ago) [57,58]. Thus, the eolian component plays a crucial role in the development of this barrier system during the mid- to late Holocene [57,58,61,63]. Overall, the middle coast of Rio Grande do Sul shows a transgressive stratigraphy with recent evidence of progradation in a few stretches [61,63]. Figures 2 and 3 shows a 500 m long processed (A) and interpreted (B) 80-MHz GPR profile perpendicular to the coast (in the vicinity of the Peixe lagoon) [60]. This interpreted stratigraphic cross section is supported by sedimentological and geochronological data [58].
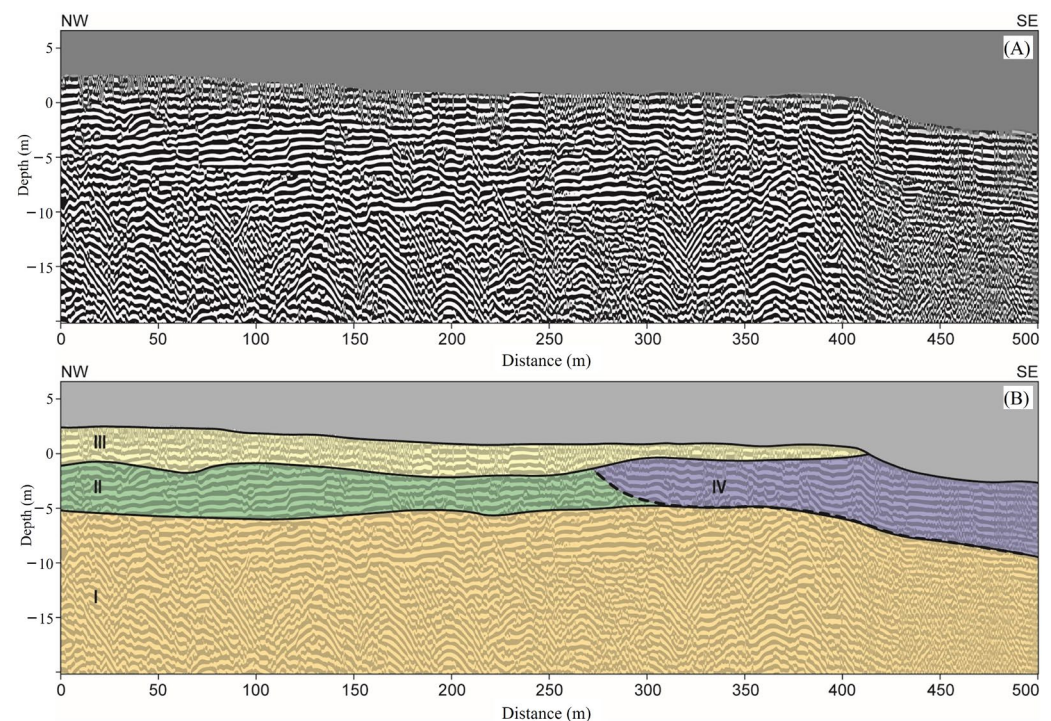
Figure 2. 2-D GPR Profile 1 from Balneário Mostardense, (**A**) processed and (**B**) interpreted. Key: I—undifferentiated deposits, corresponding to the Pleistocene substrate, II—lagoonal, III—eolian, and IV—beach (including post-beach, tidal flat, and foreshore). The dotted line marks a reversal in reflection patterns. See location in Figure 1. (Adapted from [60]).
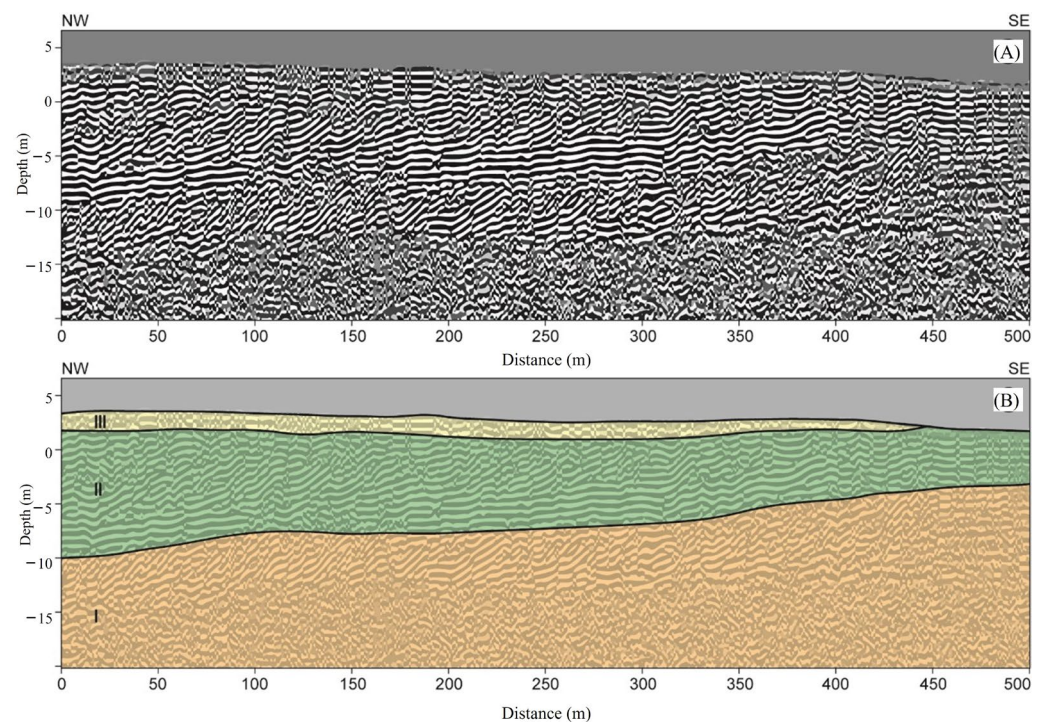
Figure 3. 2-D GPR Profile 2 from North Lagoa do Peixe, (**A**) processed and (**B**) interpreted Key: I—pre-Holocene substrate; II—lagoon margin clinoforms, and III—eolian capping. Landward to NW. See location in Figure 1. (Adapted of [60]).

3. Materials and Methods

3.1. Meteorological Data Analysis

The wind (speed and direction) and precipitation data for the study period were obtained from the Mostardas-INMET A834 meteorological station (altitude: 4 m) and provided by the Brazilian National Meteorological Institute—INMET (see location in Figure 1). This station has been operating since 13 March 2008, to 2018.

The wind data were analyzed and the rose diagram was plotted by the software GRAFER® 8.0, considering five speed classes (0–3; 3–6; 6–9; 9–12, and >12 m·s^{-1}) and the sixteen main directions of wind (N, NEN, NE, ENE, E, ESE, SE, SES, S, SWS, SW, WSW, W, WNW, NW, and NWN). They were five defined study periods for wind data analysis, in accordance with the dates of the topographic surveys: P1 (12 December 2010–7 December 2014), P2 (8 December 2014–1 April 2015), P3 (2 April 2015–20 April 2016), P4 (21 April 2016–9 December 2016), and P5 (10 December 2016–31 December 2018), with TP being (12 December 2010–31 December 2018) the total study period for the meteorological data.

For a better understanding and discussion of the results, the wind directions were subdivided into 4 quadrants: Q1 (N, NNE, NE, ENE); Q2 (E, ESSE, SE, SSE); Q3 (S, SSW, SW, WSW); and Q4 (W, WNW, NW, NNW). Furthermore, the wind directions were also classified based on their relation to the input or output of sediments in the dune system. Wind directions towards the land include NE, ENE, E, ESE, SE, SSE, S, and SSW, while wind directions towards the sea are NNE, N, NNW, WNW, W, WSW, and SW. This segmentation allows for a more precise analysis of the specific influences of these wind directions on the input or removal of sediment s in the dune field.

Monthly average rainfall and directional rainfall histograms were computed from the database of the same meteorological station. In addition, the directional histograms for the above periods were plotted considering wind direction, which allowed for identifying wind directions.

3.2. Computation of Potential Eolian Sand Transport

The first set of wind roses, for each period of dune migration analysis P1 to P5 and the total period TP, were plotted after the determination of drift potential (DP), real drift potential (RDP), and directional drift potential (DDP) according to Fryberger and Dean [64]. In these wind roses, the sand drift (SD) for each wind direction is expressed in vector units (V.U.).

Furthermore, the sand roses were computed considering the equation of Bagnold [65] for the prediction of bed load eolian sand transport, i.e., considering sediment characteristics and surface roughness too, instead of only wind characteristics as in Fryberger and Dean [64], according to Alcántara-Carrió and Alonso [66].

The empirical equation of Bagnold [65] for the prediction of eolian sand transport was utilized to calculate the potential eolian sand transport, because previous calibrations with sediment traps in the study area showed that this equation is the one that provides the best agreement with the sand transport in the area [48]. This equation considers the average grain size of sediment, the average sediment density, and the saturated air density, as well as the wind speed and direction.

The wind data were transformed to a 10 m height according to Bagnold [65]; however, the meteorological station was placed at a 4 m height. The wind values during precipitation events were considered zero, i.e., without the ability to cause eolian sand transport. The threshold wind speed used to define a transport event was defined based on the equation by Bagnold [65] to isolate the periods where there was potential for transport and exclude the remaining data. Thus, the minimum wind speed for the initiation of motion was defined as 5 m·s^{-1}, which is the minimum velocity required for sediment saltation. Therefore, only wind speeds above this velocity were considered for the sediment transport calculations. The value obtained by the equation expresses the relative amount of sand potentially transported by the wind during the time that wind was blowing. The results were compared with the previous studies in the study area and region.

3.3. Topographic Surveys

The detailed morphology and topographic evolution of five dunes from the central sectors 2 and 3 were monitored by DGPS. In sector 2, D3 and D4 correspond to barchanoid dunes; in sector 3, D5 corresponds to a barchanoid dune, while D6 and D7 are two barchan dunes (Figure 1). Six topographic surveys were carried out in December 2010 (only dunes D3 and D4), December 2014, April 2015, April 2016, December 2016, and December 2018. These surveys were performed with DGPS equipment in cinematic mode with real-time correction (RTK—real time kinematic), using a post-processed GNSS. The data were acquired using a Topcon RTK-S86T GNSS unit with the GLONASS option (datum: WGS84), having both a planar metric precision and a planar altimetric precision smaller than 1 cm.

The data processing was performed in a geographic information system using ArcMap® 10.8 software. To generate the digital terrain models (DTM), the inverse distance weighted (IDW) interpolation method was used. This method was selected for its capacity to incorporate geostatistical analyses. These analyses showed a good correlation between the measured and interpolated data, making it possible to estimate the quality of the elevation points predicted in terms of a variance estimate. The DTMs obtained through the IDW interpolation presented a very low error indicated by the distribution, even considering the differences in the number of points sampled in different years.

3.4. Remote Sensing

The satellite images were also analyzed to determine the migration of the dune crest, considering a set of 12 dunes from the four sectors of the LPNP. Thus, this remote sensing analysis was performed for the same dunes D3 to D7 from central sectors 2 and 3, monitored by DGPS topographic measurements, and seven additional dune crests: D1 and D2 from sector 1 and D8 to D12 from sector 4, in the northern and southern margin of the study area, respectively (Figure 1).

Google Earth images were employed from the available dates (July 2003; July 2005; October 2005; December 2014; December 2018). The initial images up to the year 2014 are considered interval 1, and between 2014 and 2018, they are considered interval 2. All the remote sensing products were reprojected to the UTM projection (zone 22S) and WGS84 datum. A minimum of 10 control points per image were used in the georeferencing process, and the mean squared error was less than 1.0 m. The satellite images were also georeferenced using the same control points. The use of images from Google Earth is a technique already established in several publications [67–73]. The dune slip faces and crests were used to map the dunes by photointerpretation. These morphologies correspond to light or dark linear ridges in the images, depending on the relationship between the lighting configuration (subsolar azimuth) and the trends and types of dunes [74]. Each dune was analyzed and vectorized considering these characteristics. These features were mapped using a line segment (vector data).

3.5. Determination of Dune Migration Rates

Digital terrain models (DTMs) were created based on the topographical survey data. The methodology developed by Xia and Dong [75] was utilized to determine the dune migration rates. Thus, the dune crest lines were traced over the surfaces as the lines with the highest elevation and with the greatest slip face slopes. Then, these lines were divided into points where the vectorial distance to each point was measured. The vectorial average of the points was used to obtain the average movement of the crests, as well as the migration direction. All the processing and calculations were performed in ArcMap® 10.8.

4. Results

4.1. Climate

4.1.1. Wind

The wind regime shows a multidirectional pattern with the predominance of the NE wind direction, being the secondary direction from the ENE. The landward winds are more dominant than the seaward winds, and therefore, there is an eolian sediment input blowing from the beaches to the dune fields (Figure 4 and Table 1).
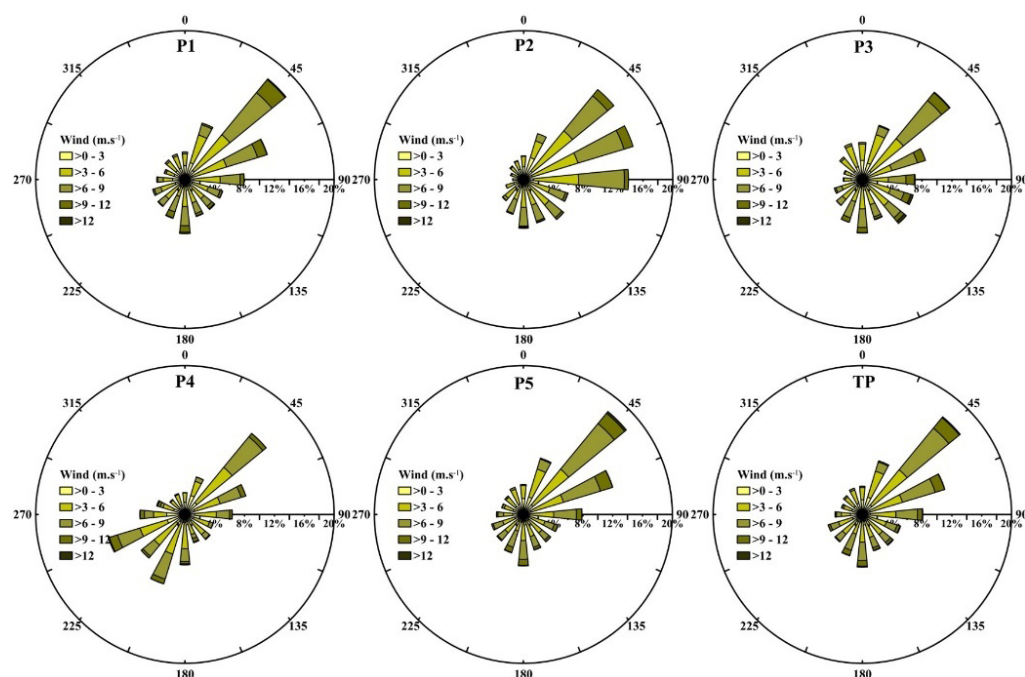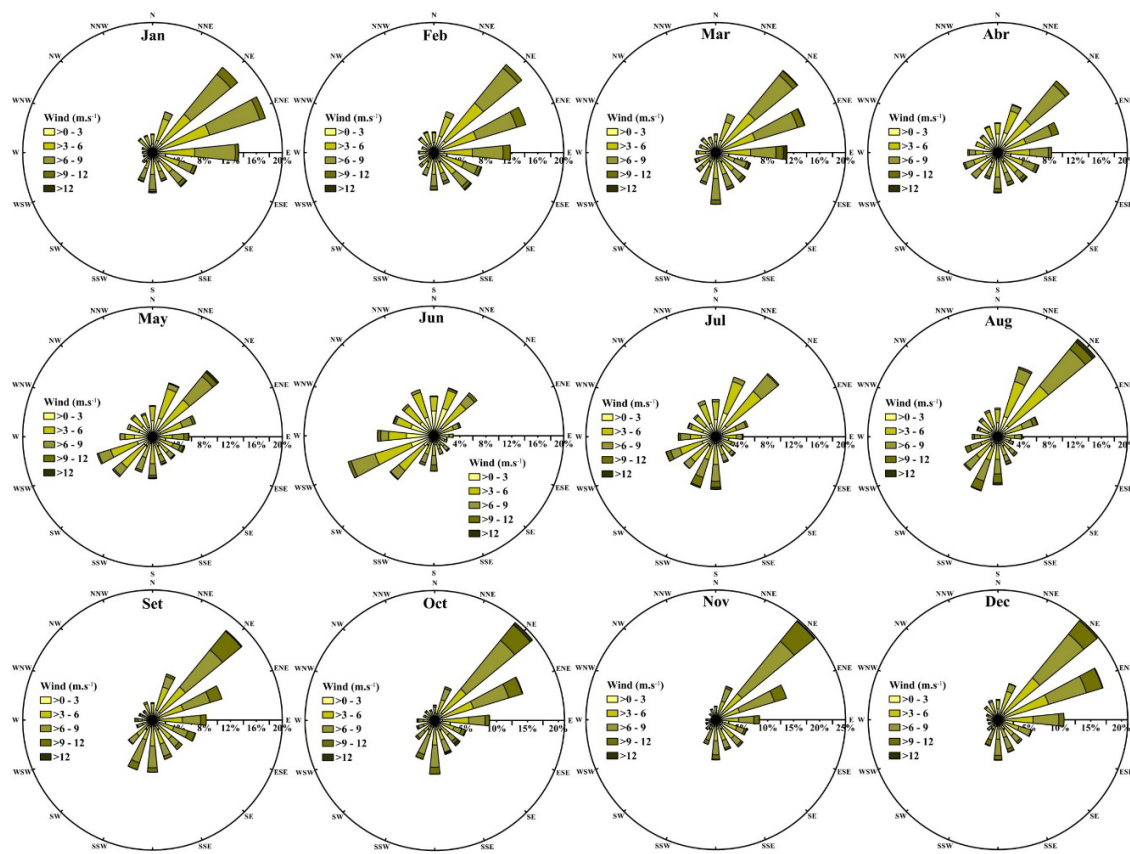

Figure 4. Wind roses by speed classes (m·s^{-1}) for the periods P1, P2, P3, P4, P5, and TP. See methodology for the temporal limits of the periods.

Table 1. The wind frequency data (%) for each direction and study period.

	N	NNE	NE	ENE	E	ESE	SE	SSE	S	SSW	SW	WSW	W	WNW	NW	NNW	Landwa	Seaward
								Wind Frequency										
P1	3.7	7.9	17.5	11.5	7.9	5.3	5.2	5.2	7.3	5.5	4.7	4.5	3.8	2.9	3.4	3.6	65.4	34.6
P2	3.2	6.5	15.7	15.3	14.1	6.2	7.0	6.1	6.6	4.9	3.7	2.5	1.5	1.8	2.4	2.7	75.8	24.2
P3	4.4	7.0	15.4	10.5	8.6	7.2	7.4	5.6	7.2	5.9	4.1	3.5	2.6	2.6	3.6	4.6	67.6	32.4
P4	2.9	5.3	14.1	8.5	6.4	4.0	4.4	4.0	6.8	9.8	7.6	10.7	6.0	4.0	2.6	2.9	57.9	42.1
P5	4.0	7.9	17.9	12.6	7.9	4.9	4.8	5.0	6.9	5.4	4.6	4.5	3.6	3.0	3.2	3.8	65.4	34.6
TP	3.8	7.5	17.0	11.6	8.1	5.4	5.4	5.1	7.1	5.8	4.8	4.8	3.7	2.9	3.3	3.7	65.5	34.5

For all periods, the landward wind directions were predominant (NE; ENE; E; ESE; SE; SSE; S; SSW), with the lowest percentage identified in P4 with 57.90% and the highest frequency of occurrence in P2 with 75.8%. The frequency of occurrence for the predominant NE wind direction ranged between 17.90% in P5 and 14.10% in P4, considering that the latter period does not include the summer season, between the months of January to March. Furthermore, this period was the only one that presented the secondary direction in WSW, with a frequency of 10.73%; in the other study periods, the secondary direction was ENE, oscillating between 15.34% and 10.47% for P2 and P3, respectively. (Figure 4 and Table 1).

The wind direction shows seasonal behavior, with the predominance of winds coming from the first quadrant (i.e., N, NNE, NE, and ENE) during the spring (October, November, December) and summer months (January, February, March). The frequencies of the winds from the third and fourth quadrants are low, with the exception of the winds from the South in October. From the end of the summer, in March, there is a gradual increase in winds from the second and third quadrants and a decrease in the frequency of winds from the first quadrant, mainly from the NE. By contrast, with the beginning of the winter, in June, the predominance of the wind's provenance is from the third quadrant Q3, with the highest frequencies from the WWS (Figure 5).

Figure 5. Wind roses by speed classes (m·s^{-1}) by months during the period 2008–2018.

The wind speed intensity also varies with the seasons, with the highest speeds from the NE between August and December, the highest speeds from the WWS direction in May and June, and the highest speeds from the S and SSW are in July and August.
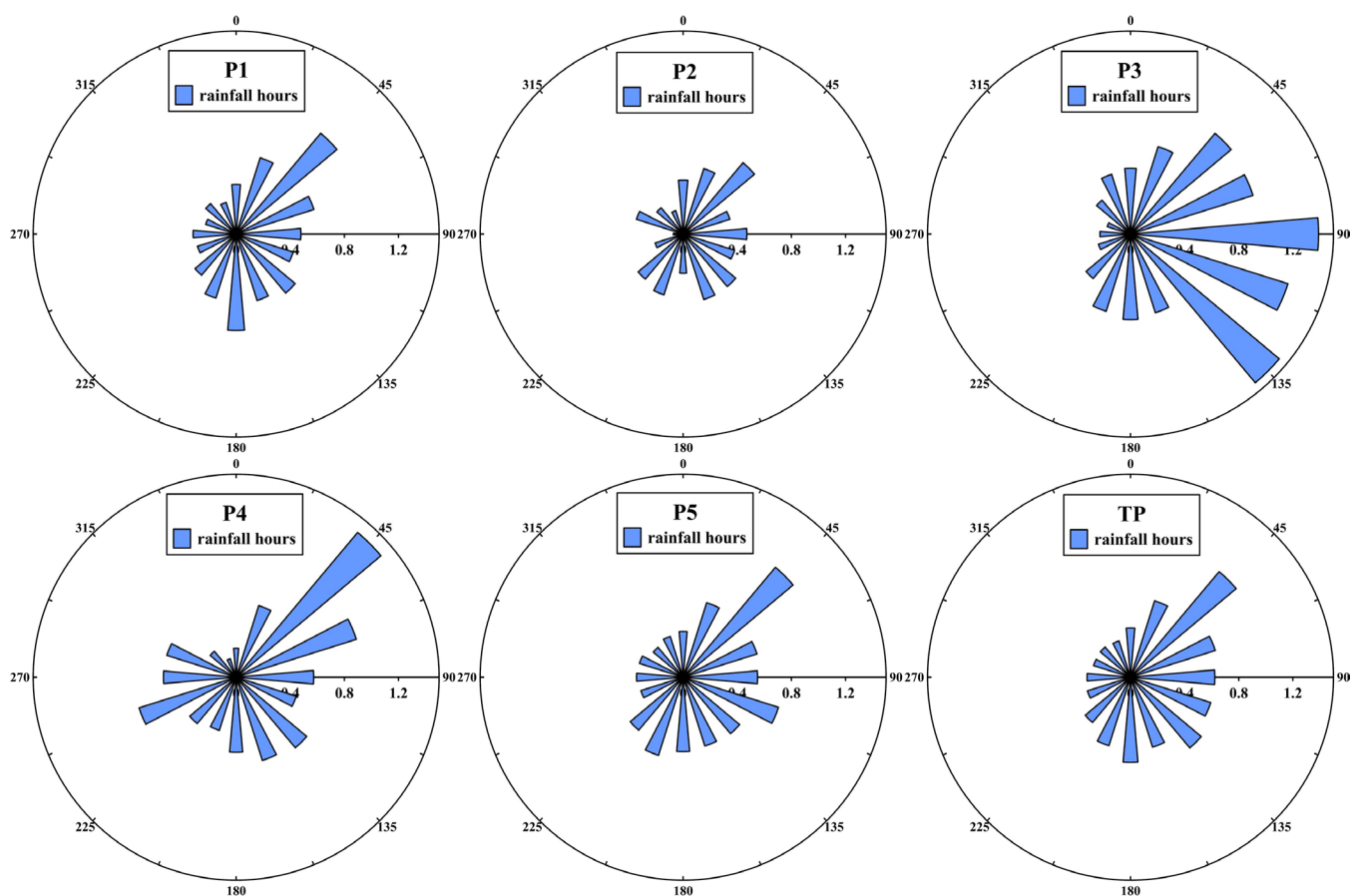
4.1.2. Rainfall

The frequency and volume of the rainfall during the study period showed great variability (Figure 6). The total annual precipitation values ranged between 966.2 (2011) and 1757.2 mm (2015), with an average of 1268.2 mm. The rainiest year was 2015, with 17% of the total precipitation of the whole study period, while the other years presented percentages between 9.5 and 12.7%.
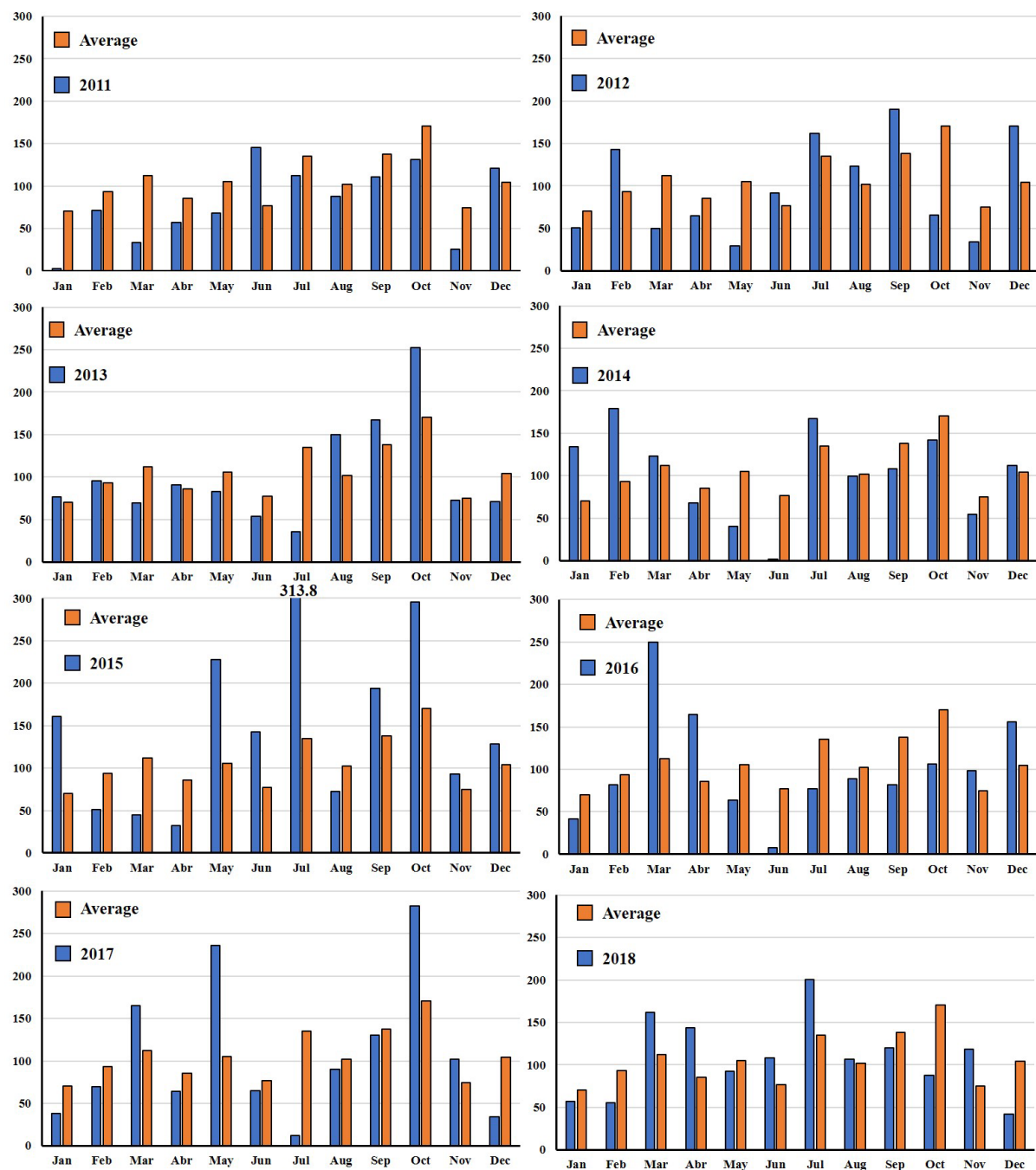
Figure 6. Tha rainfall data by month for the years between 2011 and 2018 (blue bars), compared to the average for the entire analyzed period from 2008–2018 (orange bars).

The highest precipitation volumes were associated with the winter and early spring period (June–September) and the lowest averages with the fall (March–June). The volume of precipitation showed a seasonal behavior, presenting few anomalous values to the monthly average for the entire period. In this interval of analysis, October was the month that presented the highest average precipitation (170.5 mm), with maximum values in 2015 (295.6 mm) and minimum values in 2012 (65.8 mm). The month with the highest volume of precipitation was July 2015 (313.8 mm), well above the average of 135.0 mm for this month (Figure 6). The frequency of hours with rainfall, after the wind approach direction, shows that NE winds present the highest frequency of rain, but for period P3, they were from the second quadrant (Figure 7).

Figure 7. The frequency of rainfall hours by wind direction for the analyzed periods for each analyzed period (P1 to P5) and the total period (TP).
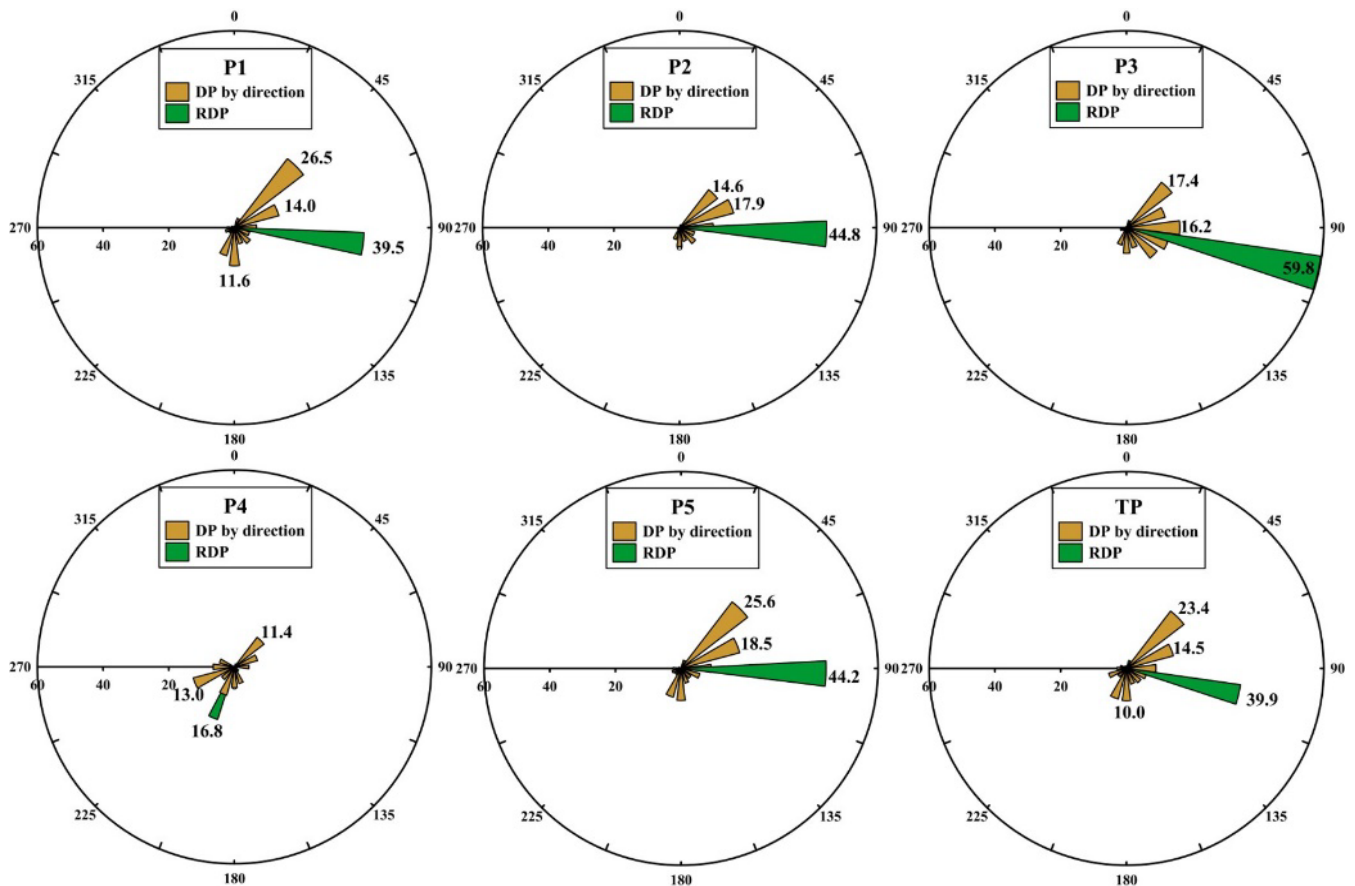
4.2. Eolian Sediment Drift Potential (Fryberger and Dean' Method)

Sand roses for each period of dune migration analysis show that the sand drift potential values are characterized by important variability. The most active period in terms of SD was P5, with values of 98.1 v.u., which is demarcating a high-energy environment. The lowest values (68.8 v.u.) were observed for period P2 (Figure 8).

The RDD for periods P1 to P3 and P5, as well as for the total study period (TP), was toward the W/WNW (Figure 8). However, the wind pattern in the fall–winter period P4 presented a significant change, with the predominance of SSW and WSW winds, and, therefore, the RDD was towards the NNE. The RDP values ranged from 16.8 (P4) to 59.8 (P3).

The wind directional variability measured through the RDP/DP ratio ranged from 0.22 (P4) to 0.65 (P2). The RDP/DP values near one indicated a unidirectional drift potential, and values near zero indicated a multidirectional drift potential. Only period P4 can be

considered low according to Fryberger and Deans' Index, indicating a high directional variability of the winds in this period. The other periods are considered intermediate. The relatively high value of 0.65 v.u. for P2 suggests that winds in this period blow predominantly from the NE/ENE quadrant, moving the sand towards the SW.


Figure 8. Potential sand transport roses for each analyzed period (P1 to P5) and the total period (TP), determined after the classical method of Fryberger and Dean (1979).

4.3. Prediction of Eolian Sediment Transport (Bagnold' Equation)

The sediment transport during the dune monitoring periods, predicted by Bagnold's equation (1941) and considering the sediment transported during rainfall events as null, shows a significant variability with a resultant direction towards W for all periods, except for P4. Thus, a very characteristic pattern is observed in periods P1–P3 and P5, where there was almost no transport associated with seaward (N–SW) winds, and most of the transport was associated with NNE/NE winds. The period P4 shows the resultant transport towards NNE/NE, i.e., an inversion in the resulting transport component. Finally, the resultant for the full period (TP) was also towards the W. The estimated values of sediment transported for the total period (TP) was 300.639 Kg·m^{-1}, the NNE/NE wind being responsible for the largest volume (maximum of 207.428) of estimated sediment transport (Figure 9).

4.4. Dune's Morphology and Migration

The morphological features of the dune system of the Lagoa do Peixe National Park present a complexity regarding the dunes dimensions. Several factors influence these features, from the sediment supply (interrupted in some sectors by anthropic activities—sector 2); the presence of vegetation, both natural and introduced; the antecedent topography of the dune system (wetlands, wind deflation zones, and blowouts); and the seasonal wind direction variation.
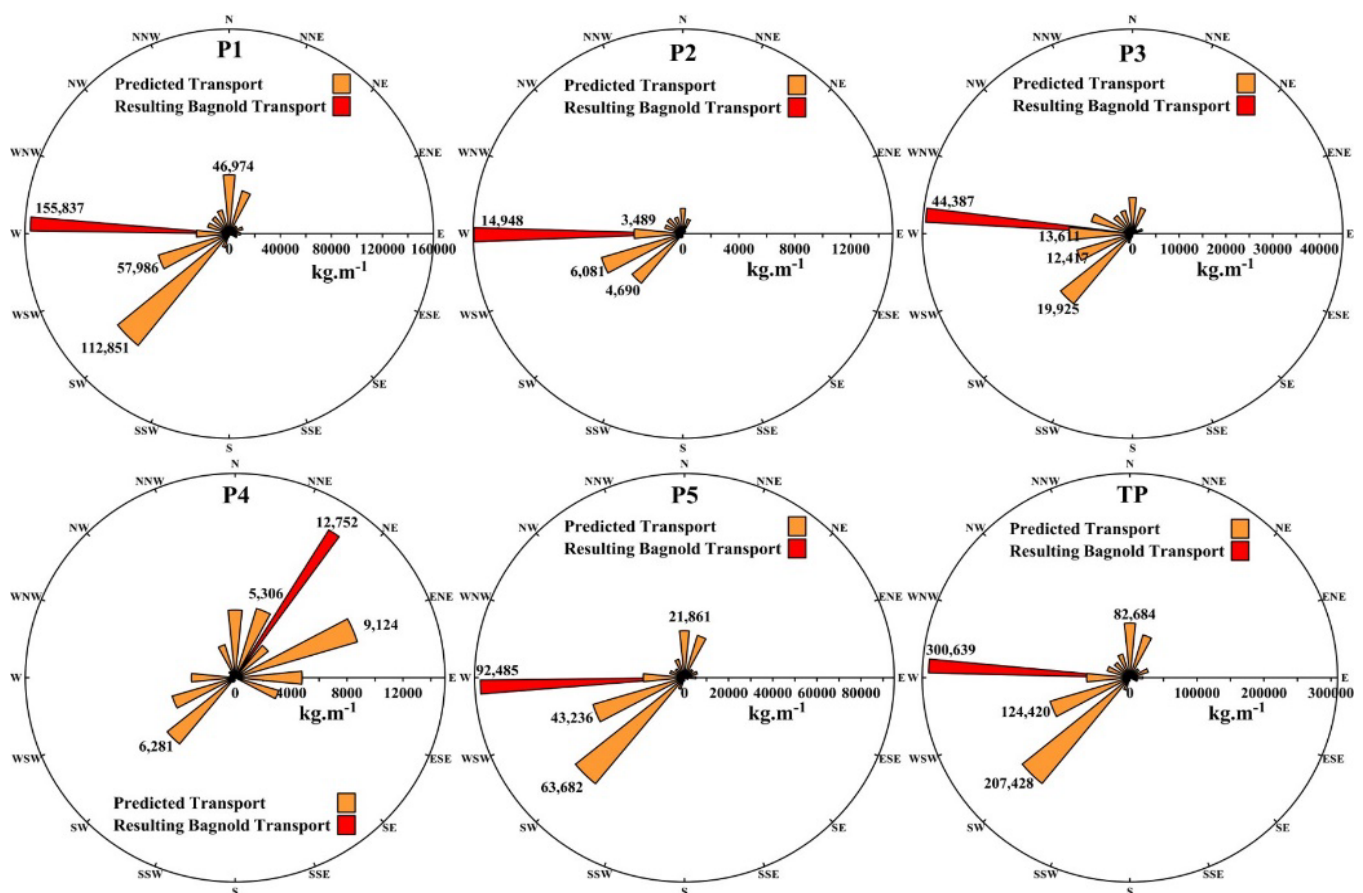
Figure 9. Modified Sand rose diagrams for the periods P1, P2, P3, P4, P5, and TP considering Bagnold' equation (1941). For each period, the prediction of the bed load sediment transport (Kg·m^{-1}) per direction is in orange and the resulting sediment transport in red.

The dune system of the LPNP is very dynamic with the continuous movement of sands, which provides constant variations in the dune dimensions. Table 2 shows the main characteristics of each dune at the beginning and at the end of the analyzed period. The maximum dune height was obtained only from the dunes monitored by DGPS. Three of these were classified as barchanoid ridges (D3, D4 and D5) and two as isolated barchan dunes (D6 and D7). As an example, the digital elevation model of dune D3 in April 2016 is shown (Figure 10).

Table 2. Morphological characteristics of the dunes at the beginning and at the end of the analyzed period. The types of the dunes were classified as isolated barchan (IB) and barchanoid ridges (BR).

|		Sector 1		Sector 2		Sector 3			Sector 4				
		D1	D2	D3	D4	D5	D6	D7	D8	D9	D10	D11	D12
Dunes features	Type	IB	IB	BR	BR	BR	IB	IB	IB	IB	IB	IB	IB
	Initial distance from the beach (m)	1459	1453	1260	1237	810	771	675	901	774	741	727	721
	Final distance from the beach (m)	1555	1650	1439	1262	915	782	870	928	917	925	861	843
	Initial width(m)	44	51	116	75	89	30	83	82	92	117	171	95
	Final width(m)	60	54	72	85	68	69	53	130	75	71	113	66
	Initial crest length(m)	325	240	453	255	297	114	216	146	184	304	268	92
	Final crest length(m)	288	162	426	239	143	150	93	196	173	168	223	118
	Maximum initial height (m)	---	---	7.1	5.0	5.5	6.5	7.5	---	---	---	---	---
	Maximum final height (m)	---	---	6.7	6.7	5.3	7.5	5.0	---	---	---	---	---
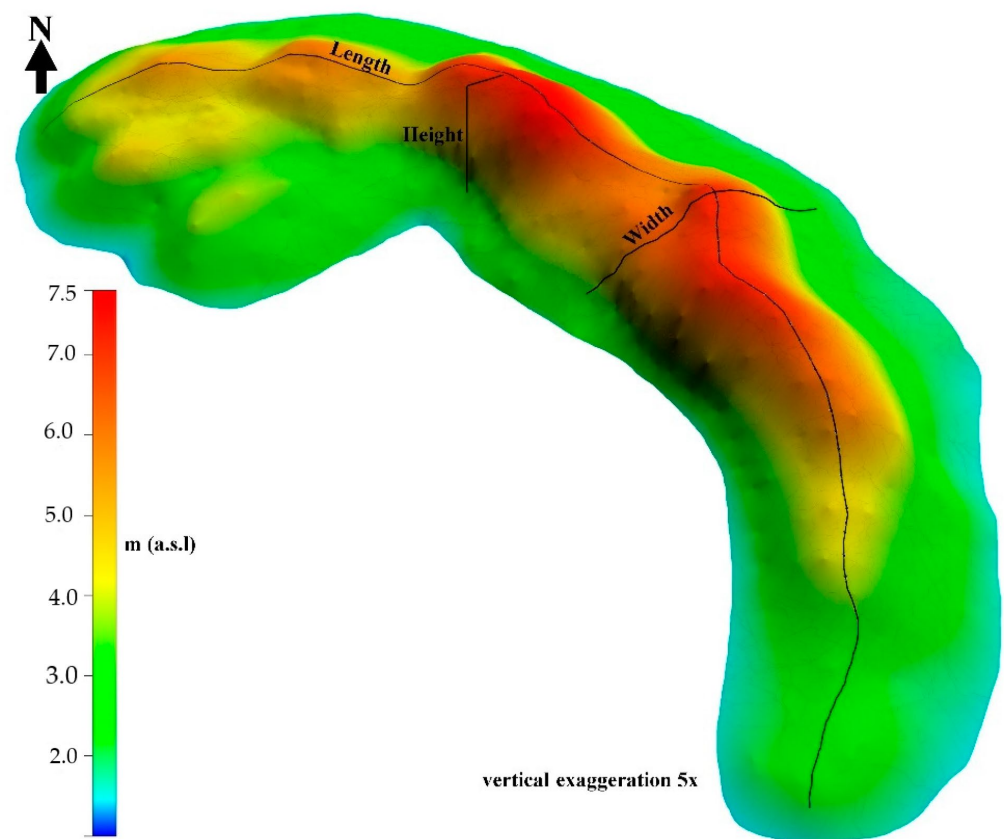
Figure 10. Example of the digital elevation model to obtain the morphological characteristics (dune D3 in April 2016). (Scale in meters above sea level; vertical exaggeration 5×).

In general, the barchanoid ridges and isolated barchan dunes showed inland migration during the sampling period, as evidenced by the increasing distances from the beach. The isolated barchan dunes showed a tendency to become narrower and shorter, whereas the barchanoid ridges showed a tendency to become narrower but with varying crest lengths (Table 2).

In sector 1, in the northern area of the PNNL, the dunes showed an increase in width and a decrease in crest length, whereas in sector 2 in the northern-central area, dune D3 reduced its width and D7 increased, with both dunes slightly decreasing their crest length, and dune D4 showed the highest growth in height, with an increment of 34%.

However, in sector 3 in the southern-central area, dune D5 (BC) was one of the dunes that showed the greatest reduction (≈50%) in crest length, while keeping its height almost stable. Furthermore, in sector 3, the two IB dunes, D6 and D7, presented the greatest discrepancies in their initial and final morphology. While dune D6 showed an increase in all parameters (width, crest length, height), dune D7 was the opposite, with decreases in all parameters. The largest increase in dune width was in D6, and the largest decrease in crest length was measured in D7. In Sector 4 in the southern area, there was a different behavior among the dunes, in which D8, located further north in this sector, showed an increase in width and crest length but, however, a smaller distance from the coast. On the other hand, the D10 dune showed the greatest reduction in crest width and length in this sector (Table 2).

The dune migration rates in sector 1 showed an important variation among the analyzed intervals of satellite images (Figure 11 and Table 3). The highest rate for dune migration was identified in the northern region of the PNNL for dune D2, with rates of 2.18 m/month (2005–2014/Interval 1), followed by 1.67 m/month (2014–2018/Interval 2). The resulting migration direction was 231° for dune crest D1 and 259° for dune crest D2.
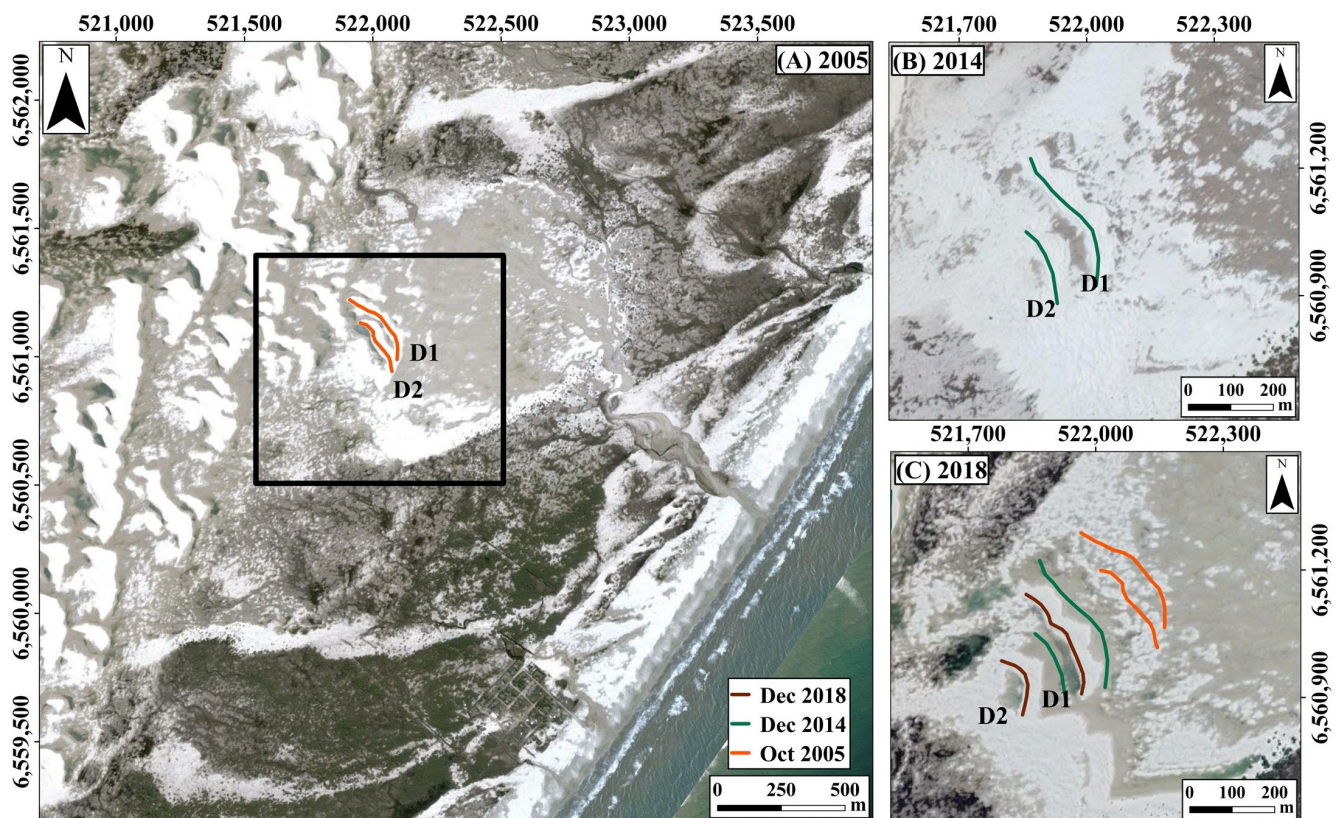
Figure 11. The migration of dunes D1 and D2 in the northern sector 1. The initial location of the dune crests in 2005 (**A**), the location of both dune crests in 2014 (**B**), and the image of 2018 with the overlay of the dune crest migration from 2005 to 2018 (**C**).

Table 3. The migration of the dune crests between interval satellite image: migration rate (m·month) and direction (°N).

|	Sector 1				Sector 2			Sector 3			Sector 4									
	D1		D2		D3		D4		D5		D6	D7	D8		D9		D10		D11		D12
Interval 1	1.67	231°	2.18	259°	1.87	263°	1.1	241°	1.31	232°			1.21	269°	1.4	270°	1.44	274°	1.88	275°	1.44	276°
Interval 2	1.38	236°	1.67	267°	1.22	284°	0.67	301°					1.00	260°	1.63	276°	1.59	262°	0.75	280°	0.73	283°

In the north central sector, both dunes (D3 and D4) presented similar initial distances from the coastline (1260 and 1237 m). However, the two dunes presented different sizes with a reasonable contrast between the initial crest widths (116 and 75 m). Similarly, the initial lengths of the crest were also different (426 and 255 m) (Table 2). During the period analyzed, the behaviors of the dunes' geomorphological changes were opposite; while D3 reduced its dimensions, D4 increased its dimensions, even with respect to the crest height (Table 2).

On the other hand, the direction and rates of migration were relatively similar, as can be seen in Figure 12 and Table 3.

However, if we analyze separately the directions and migration rates (Table 4), we will see that the crests move with some difference, especially in the periods P2 and P4. This fact may be associated with the presence of the urbanization of Mostardas beach (Figure 12).

Further south, in southern-central sector (Figure 13), D5 it was a Barchanoid Ridges (BR), demonstrated a small reduction in crest width (from 89 to 68 m) and a significant reduction in crest length, with a 50% reduction (297 to 143 m), keeping the crest height stable.
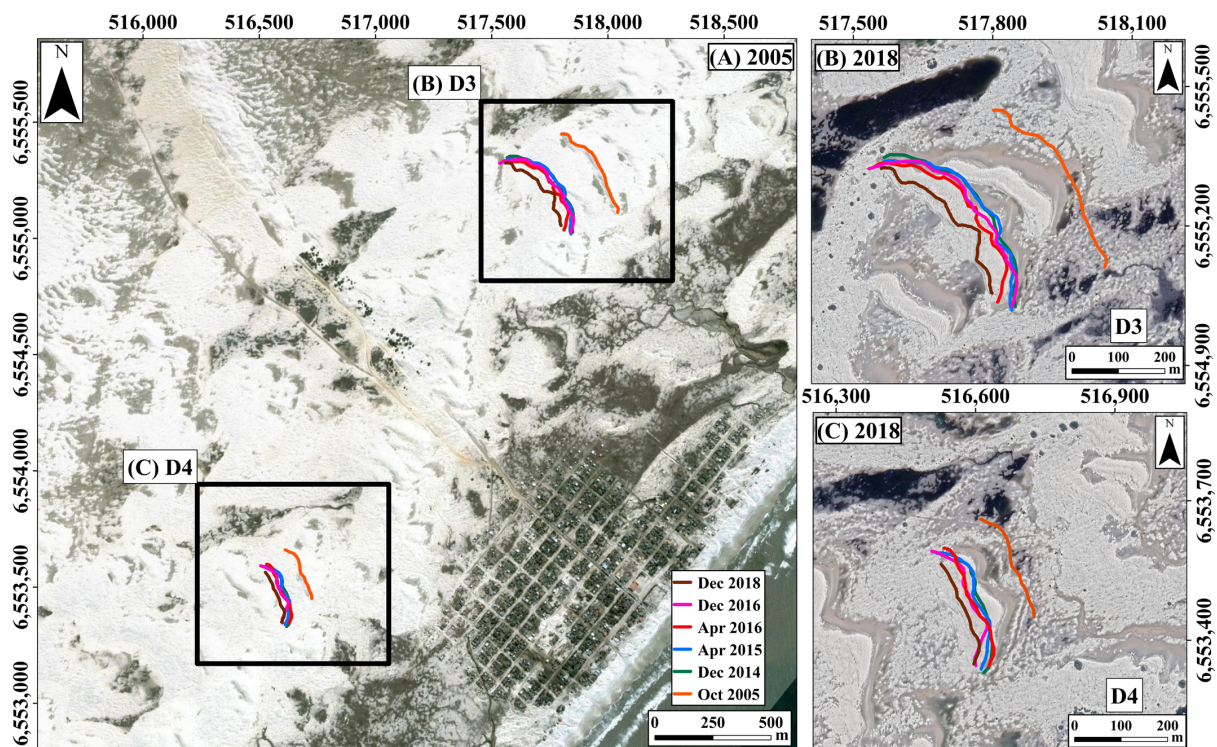
Figure 12. The migration of dunes D3 and D4 in the northern-central sector 2. (**A**) The initial location of the dune crests in 2005, and images of 2018 with the overlay of the crest migration from 2005 to 2018 of dunes D3 (**B**) and D4 (**C**), respectively.

Table 4. The migration of the dune crests between five monitoring periods: migration rate (m·month) and direction (°N).

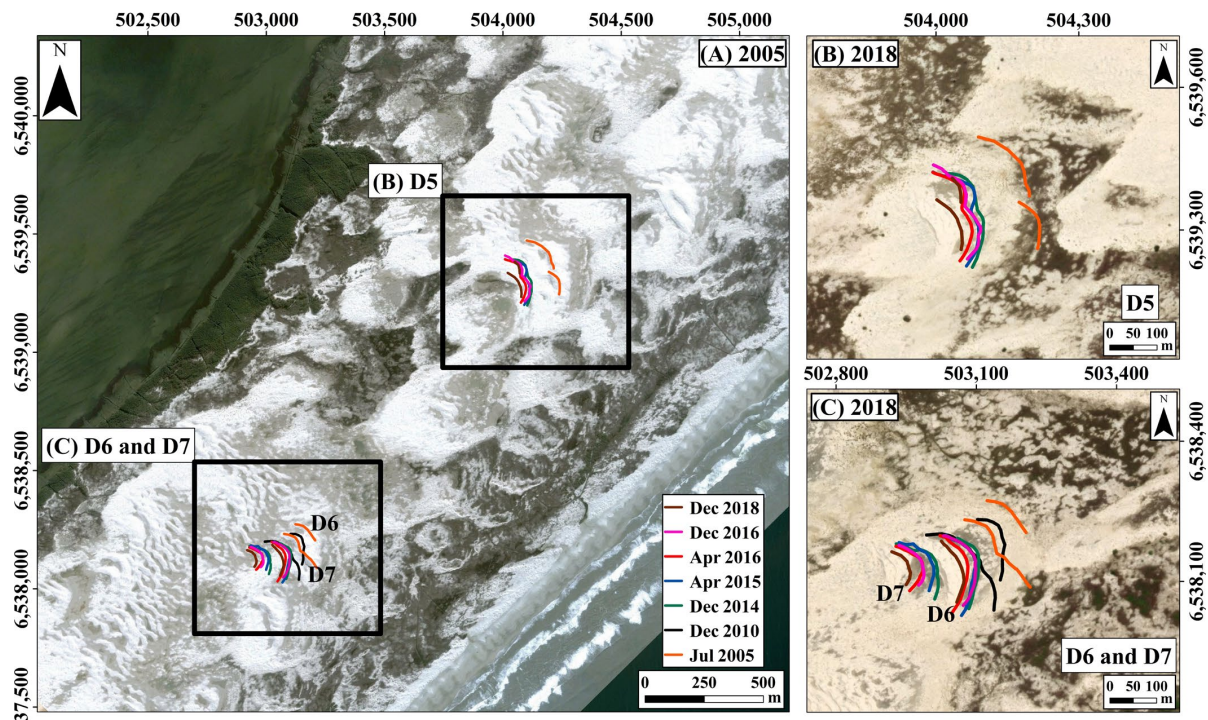|	Sector 2						Sector 3			
	D3		D4		D5		D6		D7	
P1							0.74	221°	0.81	277°
P2	0.58	207°	0.9	268°	1.76	253°	1.88	256°	1.38	290°
P3	1.36	240°	0.84	255°	1.02	267°	1.08	267°	1.42	282°
P4	1.35	61°	1.34	91°	1.10	78°	2.18	77°	2.54	63°
P5	1.02	241°	1.01	271°	0.96	260°	0.73	272°	1.17	270°

D6 and D7 are very close to each other geographically, with mutual influence on the variations of the morphological characteristics. D7 showed the biggest changes with a drastic reduction in its dimensions. It exhibited an initial distance of 675 m from the beach and a final distance of 870 m. Its initial and final widths were 83 m and 53 m, respectively. The initial ridge length was 216 m, which decreased to 93 m at the end of the sampling period. It had a maximum initial height of 7.5 m and a maximum final height of 5.0 m.

In contrast, D6 showed the greatest increments, more than doubling the crest width (from 30 m to 69 m) and increasing the crest length by 31.5% (from 114 to 150 m), as well as an increase in crest height by 1 m during the period analyzed (Table 2).

In Sector 4, south of the mouth of the Peixe lagoon, the set of 5 IB dunes behaves as an almost homogeneous set with punctual variations between each one. The morphological variations of the dune cluster are subjected to the sedimentary supply from the deflation plains between the dune cluster and the mouth of the Peixe lagoon (Figure 14). In addition, each of the dunes also provides sediment to the adjacent dunes. The direction and migration

rates of the dune cluster can be observed in Table 2, and in Figure 14, we can see the design of the dune crests at the different intervals of the satellite images.

Figure 13. Migration of the dunes D5, D6, and D7 in sector 3. The initial location of the monitored ridges in 2005 (**A**) and the images of 2008 with the overlay of the dune crest D5 (**B**), D6, and D7 (**C**) in seven stages from 2005 to 2018.
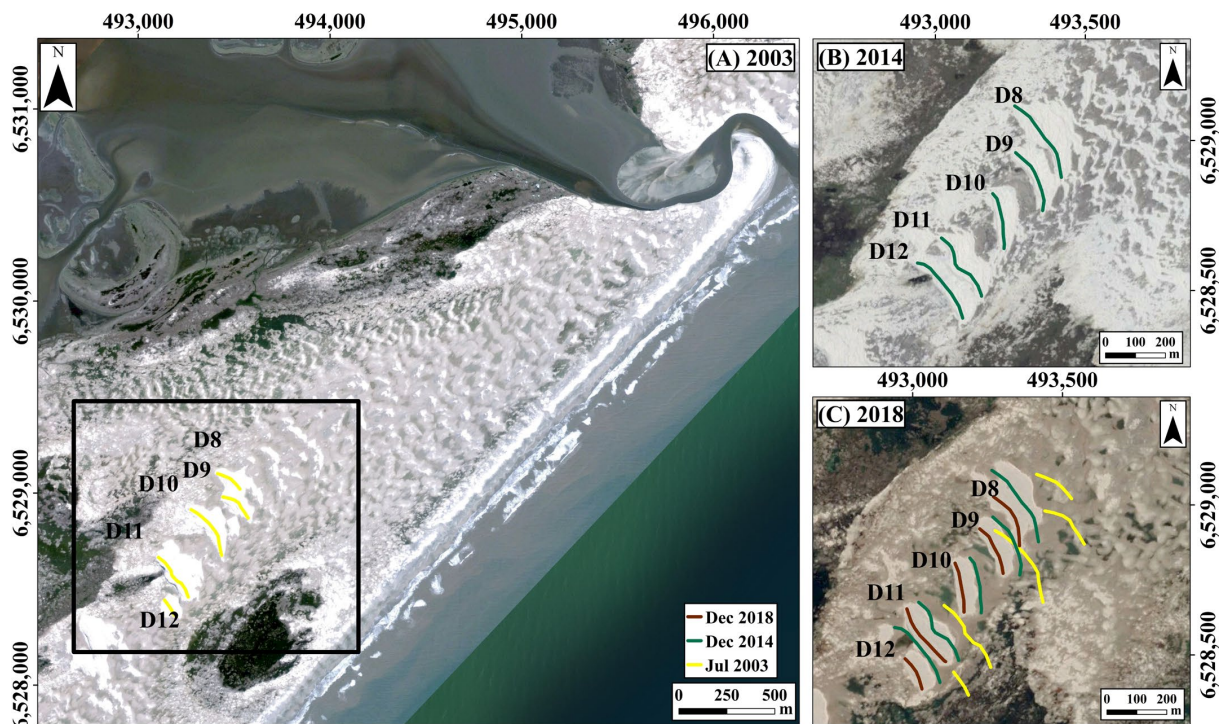
Figure 14. The migration of dunes D8 to D12 in sector 4. The initial location of the dune crests in 2003 (**A**), location in 2014 (**B**), and the image of 2018 with the overlay of the migration of dune crests from 2003 to 2018 (**C**).

The isolated barchan and barchanoid ridges dunes evidenced a complex migration pattern, with no exact parallel migration of their crests. In general, for the total study period, a westward migration was observed, showing the isolated barchanoid dunes larger displacement distances and migration rates than the barchanoid crests, while migration directions were similar, towards WSW–W (Figures 11–14).

5. Discussion

5.1. Normal Dunes Migration and Seasonal Reversion

Reverse bedforms migration is usual in bidirectional flows, i.e., waves and tides and seasonally reverse winds [76]. The reverse migration of dunes can be deduced from seasonal topographic monitoring [77] and numerical modeling [78].

The coastal plain of Rio Grande do Sul presents a high-energy wind regime (DP > 400 UV), according to the classification of Fryberger and Dean [64]. Regarding the directional variability, the low RDP/DP ratios (Table 5) reflect the obtuse bimodal characteristics of the wind regime [29], with predominant winds coming from the NE (Figure 4). The direction of the potential eolian sediment transport also evidences a high variability. The shoreline orientation of the study area is such that the NE winds transport the sediment parallel to the coast. Nevertheless, considering the direction of all the effective winds, the net eolian sediment transport in an annual scale is toward the WNW–W (Figures 8 and 9).

Field monitoring in the study area facilitated the observation of a reversal in the direction of dune migration. The direction of the migration of the dune crests during the entire study period (December 2010–December 2018) was towards WSW–W, which is consistent with the regional dune dynamics (RDD), morphological configuration, and the overall migration of the dune field, as depicted in Figure 4 and Table 4. This trend was also observed during periods P1, P2, P3, and P5. However, from April to December 2016, the dune crests migrated towards ENE–E, as shown in Figure 4 and Table 4, and the RDD changed to NNE (Figures 8 and 9). Therefore, there was a significant change in both the potential eolian sediment transport and the actual dune migration during period P4, albeit not in the same direction.

The normal dune migration and seasonal reversion are a phenomenon observed in various regions worldwide. Reversing transverse dune migration is associated with bimodal seasonal wind regimes [77–81] and so are relatively rare eolian bedforms [78]. Reversing migration has been described for transverse dunes oriented normal to the shoreline [78], desert linear dunes [82], continental barchan dunes [83], and linear coastal dunes [10].

Similar to the coastal plain of Rio Grande do Sul, reversing dune migration was reported at the Mpekweni site in South Africa [78]. The study used 3D computational fluid dynamic modeling to examine the behavior of the near surface airflow traveling over transverse (reversing) dunes on a beach system. When the wind direction is reversed, the dune morphology is rapidly modified, particularly at the dune crests, where rounding and aerodynamic smoothing takes place. The study provides detailed insights into how 3D airflow behavior is modified according to the incident flow direction of reversing dune ridges and the resulting implications for their topographical modification.

The Itapeva dune field, situated in Brazil, presents inverted dunes characterized by major and minor slip faces oriented in opposing directions. This research emphasizes the significance of regional geomorphology in altering local wind patterns and its consequent influence on dune dynamics. Continued monitoring of the dunes has revealed the occurrence of simultaneous slip faces oriented in different directions within the dune field [84].

The reversion of the dune migration direction during P4 reveals the contribution of the effective SSW–WSW winds for the sediment transport. The presence of cold fronts, more frequently in winter, generates extreme SSW–WSW winds [85,86], and therefore, the cold fronts can be considered responsible for the reversion of the migration direction of the transgressive barchan and barchanoid dunes. As reported by Machado and Calliari [86],

between 1948 and 2013, there was an increase in extreme wind events coming from the SW quadrant. Therefore, this increase can result in a decreasing trend of the net migration rates for the transgressive dunes and, consequently, an apparent stabilization. Coastal dune stabilization is related to an increase in climate changes or human activities and the consequent increase in vegetal cover [13,87,88]. On the other hand, Costas and co-workers [89] suggest that vegetation plays a passive role with respect to topography, and external agents: sediment supply, beach width, and wind intensity, are much more effective. However, several environmental factors may lead to periods of dune field stabilization, such as climatic variations in precipitation (including the role of groundwater fluctuations), changes in the wave and wind regime, sea level variations, shoreline erosion, grazing activities, and sediment supply, as well as the influence of exotic flora and fauna [90].This study shows that the increase in reversing migration, due to changes in seasonal wind patterns, i.e., the increase in polar fronts in the study area, is another factor that can contribute to coastal dune stabilization. Conceptual models of the evolution of transgressive dune field systems [91] might also include this reverse migration.

Wind energy is frequently considered one of the main controlling factors over dune activity in areas where there is low human activity [92]. In the Peixe lagoon dune field, given the lack of urbanization, the dunes migrate according to the influence of the prevailing winds.

Rain precipitation is another factor that controls the dune migration, due to humidity avoidance or difficult sediment transport [93]. The different direction between the potential eolian sediment transport and the effective dune migration can be an effect of precipitation associated with cold fronts. Theoretically, the sediment transport should be considered negligible during rainfall events [94]. However, the intensity of SSW–WSW winds suggests that during precipitation events (Figure 7) or after a fast desiccation of sand, due to the absence of grass or other vegetation in the dunes, the eolian sediment transport can be produced, in accordance with the studies of Logie [95] and Sarre [96].

The dune field is wider in the northern sector of the study area, the barchanoid dunes are more abundant and the barchan dunes present higher dimensions. Therefore, a higher availability of sediments for the northern sector can be deduced, in accordance with a higher volume of eolian sediments [11]. The net annual eolian sediment transport is landward and, therefore, the eolian flux of sediments between both sectors is negligible. It implies that this higher availability of sediments in the northern sector must be only related to the input of sediments from the beaches. The shoreline orientation shows a small progradation or cuspate morphology in the northern sector, if compared with the general shoreline orientation in the region (Figure 1). Therefore, it can imply a higher concentration of wave energy in the northern sector of the study area, inducing a more dissipative stage of the beach, which favors a higher input of eolian sediments and the better development of dunes, according to the criteria of Short and Hesp [6]. The little changes in the shoreline orientation control the local variability in the eolian sediment availability and, consequently, the distribution and height of barchan and barchanoid dune types, as well as the location of the Peixe lagoon in the southern sector.

5.2. Dune's Migration Trends for the Coastal Plain of Rio Grande do Sul

Several studies have described the eolian potential drift (RDP, RDD) and migration rates of dunes in the coastal plain of Rio Grande do Sul (Table 4), despite only two of them [29,97] conducting direct field measurements.

Tomazelli [29] analyzed the wind regime and the dune migration rates in the northern region of the CPRGS. In total, the wind data series comprised 13 years, from January 1970 to December 1982. This study suggests a resultant drift direction (RDD) to SW (220°N) due to the large predominance of NE and E winds, associated with the edge of the South Atlantic Anticyclone. The analysis of the drift potential data revealed a large seasonal variation, which is a result of changes in the wind regime of this coastal region. According to the author, during fall and winter (i.e., from April to August), there is a reduction in the drift potential and a significant change in the drift direction, which, due to the predominance of

winds coming from W and SW, practically reverses its direction. During spring–summer, drift potential increases (average November value: 203.9 UV) and the drift direction returns to its regular orientation, towards SW. The analysis of aerial photographs and satellite images, for a total period of 27 years, was conducted on different dune morphological types and revealed annual average rates between 10 and 38 m·yr^{-1} (Table 4). Direct field measurements conducted on a barchanoid dune with an average height of 8 m over three years showed an average migration rate of approximately 26 m·yr^{-1} in the SW direction (230°N) [29].

Table 5. The comparative table for real potential drift (RDP), resultant drift direction (RDD), migration rates (m/year) and kind of dunes for several dune fields in the coastal plain of Rio Grande do Sul.

	Region	Period of Study	RDP (UV)	RDD	Migration Rate (m·yr^{-1})	Type of Dune	Author
Northern Coast	Torres	1970–1982	800	WSW	-	-	[29]
	Torres	1970–1982	±23	NW	-	-	[58]
	Torres	2008–2015	4.65	-	-	-	[98]
	Tramandaí	2003–2005	±55	SW	-	-	[58]
	Tramandaí	2008–2015	50.85	-	-	-	[98]
	Imbé	1970–1982	1442	SW	-	-	[29]
	Imbé	1948–2003	±44	SW	-	-	[58]
	Magisterio, Pinhal	1986–1989	-	SW	26	Barchanoid	[29]
	Magisterio, Pinhal	1974–1987	-	SW	14.7	Parabolic	[34]
	Magisterio, Pinhal	1974–1987	-	SW	24	Barchan	[34]
	North/middle Coast	1948–1967	-	SW	14.0	Barchan	[29]
	North/middle Coast	1967–1974	-	SW	11.0–32.0	Barchanoid	[29]
Middle coast	Dunas Altas, Palmares do Sul	1987–1999	-	SW	22.5	Parabolic	[34]
	Dunas Altas, Palmares do Sul	1987–1999	-	SW	28.0	Barchanoid	[34]
	Mostardas	1957–2000	±45	W	-	-	[58]
	Peixe lagoon	2010–2018	99.4	WSW-W	16.55	Barchan/Barchar	Present study
	Rio Grande	1970–1982	409	W	-	-	[29]
Southern coast	Taim	2003	57.57	ENE	0	Barchan	[97]
	Taim	2004	103	N	0	Barchan	[97]
	Taim	2005	105.2	NW	20	Barchan	[97]
	Chuí	2003–2006	±90	NWN	-	-	[34]

Guimarães [97] studied the migration of a barchan dune on the southern sector of CPRGS between 2003 and 2005. During 2003, the direction remained between E–NE, while between 2004 and 2005, it changed to NNE. Significant dune migration was not registered between 2003 and 2004, only variations in volume, orientation, and height. However, during 2005, the dune migrated 20 m to the NW and W. According to the author, there is larger wind direction variability in this sector region when compared to other areas of the CPRGS. The author highlights that the years of 2004 and 2005 were atypical, including the Catarina Hurricane (the only hurricane registered in the state).

Another important study in regional scale was conducted by Martinho [34]. DP and RDP variations were analyzed on the northern and middle sectors of CPRGS. Dune migration analyses were also conducted using aerial photographs (1948, 1974, and 1989) and LANDSAT satellite images (1980, 1987, and 1999, with resolutions of 60, 30, and 15 m, respectively). This study identified dune migration rates ranging from 14.7 to 28 m·yr^{-1}, with a direction between 214 and 234°N (Table 3).

When comparing the real drift potential (RDP) between studies, it is possible to see a large discrepancy of results, even though the same method of Fryberger and Dean [64] was used. On the other hand, the resultant drift direction (RDD) results are very similar. Overall, all authors emphasize an RDP reduction from the southern and middle sectors to the northern sector, the last one represented by the Torres dune field. According to Martinho [34], the winds on the northern sector are less strong when compared to the middle sector of the CPRGS, resulting in smaller values of RDP. The NE winds blow

parallel to the coast, with its corridor limited by the Serra Geral escarpments. On the other hand, in the middle sector, the winds are stronger and present larger RDP values; in this sector the winds reach the coast at an oblique angle and have a larger wind corridor due to the gentle topography of the coastal plain. In the middle sector, the RDD ranges from SW to W. This sector presents a larger range of wind directions, even though the winds from NE and S are stronger and more important. The south sector has a larger variability in wind direction, presenting an annual average toward WSW but also periods with eolian sediment transport to the north. As demonstrated by Guimarães [97] and the present study, a short-term analysis demonstrates that the migration rates are not constant over the years and can result in null or reverse migrations because of the seasonal wind variations.

The RDP values must be interpreted as representative of the wind energy for each sector. The efficiency of the eolian sand transport depends also on the local characteristics of the surface over which the wind acts. Therefore, the RDP values are not necessarily equal to the real drift, since local characteristics inherent to the terrain surface (topographic variations, humidity levels, grain sizes, and presence of vegetation) over where the wind blows can affect the amount of sand that is effectively transported [29,64].

Considering the effective winds for the dunes formation and their migration rates, a reduction in wind speed and prevailing direction can result in reduced transport and stabilization of the dune field. The analysis of the Imbé meteorological station shows interdecadal variations on the RDP: it decreased between 1948 and 1955, significantly increased between 1955 and 1964, continually decreased from 1964 to 1988, and a short increase occurred from 1988 to 2003 [58]. Similarly, the historical series of meteorological data show a decrease in the monthly average wind speed and an increase in precipitation since 1961 at the extreme north of the CPRGS [99].

The dune migration rates presented by [29,34], obtained from satellite images between 1948 and 1987, can be considered relevant on a large-scale context of dune field changes. However, these results no longer reflect the current migration rates, given that these fields have suffered significant changes and stabilization processes. By contrast, in 1948, for example, the Torres and Mostardas dune fields were completely active without vegetation or deflation areas.

6. Conclusions

The climate data were analyzed to depict trends in dune behavior. The SW–NE shoreline orientation of the study area generates NE winds, which are the most frequent and carry sediments parallel to the coast. Nevertheless, considering the multidirectional wind directions during the year, the resultant drift direction is WSW–W, which generates a net annual input of sediments landward.

The slightly cuspate shoreline of the northern sector induces a more dissipative stage of the beaches and a higher input of sediments to the dune field. Consequently, there is a higher availability of sediments, evidenced by a higher development of barchanoid and barchan dunes with higher dimensions and a wider extension of the dune field in the northern sector. Altogether, this determines the location of the Peixe lagoon in the southern sector of the study area.

The annual average dune migration rates ranged from xx–xx (Barchan) and xx–xx (Barchanoid). The dune crest migrations in the dune field close to the Peixe lagoon show average rates of 16.55 m·year^{-1} for dunes. The predominant direction of migration for both types of dunes is towards WSW–W. This dune crest migration is mainly controlled by the direction of the effective winds due to the absence of vegetation in the dune field and the lack of urbanization in the national park. These dune migration patterns are in agreement with both the sediment transport calculations and the geomorphological configuration of the transgressive dune field.

The seasonal reversion of dune migration occurs during occasional periods. The seasonal analysis shows the relevance of the effective SSW–WSW winds for the sediment transport, dune migration, and dune field stabilization. The past cold fronts closest to Rio

Grande do Sul generate these intense winds and, consequently, a reversion in the migration direction of the barchan and barchanoid dunes, changing it to migrate towards the NNE. This reversion is coherent with the reversion in the direction of the eolian sediment transport indicated by the previous studies, based on the calculation of wind drift potential. This result warns of the possibility of a reduction in the migration rates of the transgressive dunes, due to both the tendency to increase the occurrence of extreme events and the greater entry of cold fronts in this sector of the RS coast.

Consequently, the identified reverse migration of dunes explains the stabilization of the dune fields at CPRGS. The decrease in both speed and frequency of prevailing winds results in reduced transport and stabilization of the dune field. Therefore, reverse dune migration results in a factor controlling dune stabilization and the geomorphological evolution of transgressive coastal dune fields.

The implications of our research extend beyond the local level and have wider international implications. The coastal dune fields are valuable ecosystems around the world that serve as natural barriers against coastal erosion, protect coastal communities, and provide critical habitats for numerous plant and animal species. Understanding the dynamics of dune behavior and the factors influencing their migration and stability is critical for effective coastal management and adaptation strategies in the face of ongoing climate change. By elucidating the complex interplay between wind patterns, sediment transport, and dune morphology, our findings contribute to a better understanding of coastal systems and may inform decision-making processes for the conservation and sustainable management of these fragile coastal environments.

References

1. Martinez, L.L.; Psuty, N.P. *Coastal Dunes, Ecology and Conservation. Ecological Studies*; Springer: Berlin/Heidelberg, Germany, 2004; Volume 171.
2. Hesp, P.A.; Martínez, M.L. Disturbance Processes and Dynamics in Coastal Dunes. In *Plant Disturbance Ecology*; Elsevier: Amsterdam, The Netherlands, 2007; pp. 215–247.
3. Davidson-Arnott, R.G.D.; Law, M.N. Seasonal Patterns and Controls on Sediment Supply to Coastal Foredunes. Long Point, Lake Erie. In *Coastal Dunes: Form and Process*; Nordstrom, K., Psuty, N., Carter, R.W.G., Eds.; Wiley: New York, NY, USA, 1990; pp. 117–200.
4. Packham, J.R.; Willis, A.J. *Ecology of Dunes, Salt Marsh and Shingle*; Springer: New York, NY, USA, 1997; ISBN 978-0-412-57980-6.
5. Walker, I.J.; Davidson-Arnott, R.G.D.; Bauer, B.O.; Hesp, P.A.; Delgado-Fernandez, I.; Ollerhead, J.; Smyth, T.A.G. Scale-Dependent Perspectives on the Geomorphology and Evolution of Beach-Dune Systems. *Earth-Sci. Rev.* **2017**, *171*, 220–253. [CrossRef]
6. Short, A.D.; Hesp, P.A. Wave, Beach and Dune Interactions in Southeastern Australia. *Mar. Geol.* **1982**, *48*, 259–284. [CrossRef]
7. Bird, E.C.F. Coasts. In *An Introduction to Systematic Geomorphology. Australian National*; Australian National University Press: Canberra, Australian, 1976.

8. Hesp, P.A. The Beach Backshore and Beyond. In *Handbook of Beach and Shoreface Morphodynamics*; Short, A.D., Ed.; John Wiley and Sons Ltd.: Hoboken, NJ, USA, 1999; pp. 145–270.

9. Goldsmith, V. Coastal Dunes. In *Coastal Sedimentary Environments*; Davis, R.A., Ed.; Springer: Berlin/Heidelberg, Germany, 1978; pp. 171–235.

10. Alcántara-Carrió, J.; Alonso, I. Aeolian Sediment Availability in Coastal Areas Defined from Sedimentary Parameters. Application to a Case Study in Fuerteventura. *Sci. Mar.* **2001**, *65*, 7–20. [CrossRef]

11. Fontán Bouzas, A.; Alcántara-Carrió, J.; Montoya Montes, I.; Barranco Ojeda, A.; Albarracín, S.; Rey Díaz de Rada, J.; Rey Salgado, J. Distribution and Thickness of Sedimentary Facies in the Coastal Dune, Beach and Nearshore Sedimentary System at Maspalomas, Canary Islands. *Geo-Mar. Lett.* **2013**, *33*, 117–127. [CrossRef]

12. Xu, Z.; Mason, J.A.; Lu, H. Vegetated Dune Morphodynamics during Recent Stabilization of the Mu Us Dune Field, North-Central China. *Geomorphology* **2015**, *228*, 486–503. [CrossRef]

13. Anthonsen, K.L.; Clemmensen, L.B.; Jensen, J.H. Evolution of a Dune from Crescentic to Parabolic Form in Response to Short-Term Climatic Changes: Råbjerg Mile, Skagen Odde, Denmark. *Geomorphology* **1996**, *17*, 63–77. [CrossRef]

14. Tsoar, H.; Blumberg, D.G. Formation of Parabolic Dunes from Barchan and Transverse Dunes along Israel's Mediterranean Coast. *Earth Surf. Process. Landf.* **2002**, *27*, 1147–1161. [CrossRef]

15. Yizhaq, H.; Ashkenazy, Y.; Tsoar, H. Why Do Active and Stabilized Dunes Coexist under the Same Climatic Conditions? *Phys. Rev. Lett.* **2007**, *98*, 98–101. [CrossRef]

16. Yizhaq, H.; Ashkenazy, Y.; Tsoar, H. Sand Dune Dynamics and Climate Change: A Modeling Approach. *J. Geophys. Res. Earth Surf.* **2009**, *114*, 1–11. [CrossRef]

17. Lavee, H.; Imeson, A.C.; Sarah, P. The Impact of Climate Change on Geomorphology and Desertification along a Mediterranean-Arid Transect. *Land Degrad. Dev.* **1998**, *9*, 407–422. [CrossRef]

18. Lancaster, N. Eolian Features and Processes. In *Geological Monitoring*; Young, R.N., Ed.; Geological Society of America: Boulder, CO, USA, 2009; pp. 1–25.

19. Bigarella, J.J.; Klein, A.H.D.F.; Menezes, J.T.; Vintém, G. Sub-Tropical Coastal Dunes: Examples from Southern Brazil. *J. Coast. Res.* **2005**, *42*, 113–137.

20. Hernández-Calvento, L.; Jackson, D.W.T.; Medina, R.; Hernández-Cordero, A.I.; Cruz, N.; Requejo, S. Downwind Effects on an Arid Dunefield from an Evolving Urbanised Area. *Aeolian. Res.* **2014**, *15*, 301–309. [CrossRef]

21. Bailey, S.D.; Bristow, C.S. Migration of Parabolic Dunes at Aberffraw, Anglesey, North Wales. *Geomorphology* **2004**, *59*, 165–174. [CrossRef]

22. Madole, R.F. Spatial and Temporal Patterns of Late Quaternary Eolian Deposition, Eastern Colorado, U.S.A. *Quat. Sci. Rev.* **1995**, *14*, 155–177. [CrossRef]

23. Jimenez, J.A.; Maia, L.P.; Serra, J.; Morais, J. Aeolian Dune Migration along the Ceará Coast, North-Eastern Brazil. *Sedimentology* **1999**, *46*, 689–701. [CrossRef]

24. Girardi, J.D.; Davis, D.M. Parabolic Dune Reactivation and Migration at Napeague, NY, USA: Insights from Aerial and GPR Imagery. *Geomorphology* **2010**, *114*, 530–541. [CrossRef]

25. Miot da Silva, G.; Hesp, P.A. Increasing Rainfall, Decreasing Winds, and Historical Changes in Santa Catarina Dunefields, Southern Brazil. *Earth Surf. Process. Landf.* **2013**, *38*, 1036–1045. [CrossRef]

26. García-Romero, L.; Hesp, P.A.; Peña-Alonso, C.; Miot da Silva, G.; Hernández-Calvento, L. Climate as a Control on Foredune Mode in Southern Australia. *Sci. Total Environ.* **2019**, *694*, 133768. [CrossRef]

27. Hansen, E.; DeVries-Zimmerman, S.; van Dijk, D.; Yurk, B. Patterns of Wind Flow and Aeolian Deposition on a Parabolic Dune on the Southeastern Shore of Lake Michigan. *Geomorphology* **2009**, *105*, 147–157. [CrossRef]

28. Bristow, C.S.; Lancaster, N. Movement of a Small Slipfaceless Dome Dune in the Namib Sand Sea, Namibia. *Geomorphology* **2004**, *59*, 189–196. [CrossRef]

29. Tomazelli, L. O Regime Dos Ventos e a Taxa de Migração Das Dunas Eólicas Costeiras Do Rio Grande Do Sul, Brasil. *Pesquisas em Geociências* **1993**, *20*, 18. [CrossRef]

30. de Souza Matos-Carneiro, M.; Ferreira, B.; Gregorio, M.; Pessanha, P.; Lins da Silva, D.; de Oliveira-Vital, S. Datos Espaciales LIDAR En La Caracterización Geomorfológica Del Campo de Dunas Costeras Del Río de Fogo, Río Grande Do Nort—Brasil. *Rev. Geográfica De América Cent.* **2018**, *2*, 315–348. [CrossRef]

31. Pickart, A.J.; Hesp, P.A. Spatio-Temporal Geomorphological and Ecological Evolution of a Transgressive Dunefield System, Northern California, USA. *Glob. Planet. Chang.* **2019**, *172*, 88–103. [CrossRef]

32. Ruessink, B.G.; Arens, S.M.; Kuipers, M.; Donker, J.J.A. Coastal Dune Dynamics in Response to Excavated Foredune Notches. *Aeolian. Res.* **2018**, *31*, 3–17. [CrossRef]

33. Andriolo, U.; Gonçalves, G.; Sobral, P.; Fontán-Bouzas, Á.; Bessa, F. Beach-Dune Morphodynamics and Marine Macro-Litter Abundance: An Integrated Approach with Unmanned Aerial System. *Sci. Total Environ.* **2020**, *749*, 141474. [CrossRef] [PubMed]

34. Martinho, C.T.; Hesp, P.A.; Dillenburg, S.R. Morphological and Temporal Variations of Transgressive Dunefields of the Northern and Mid-Littoral Rio Grande Do Sul Coast, Southern Brazil. *Geomorphology* **2010**, *117*, 14–32. [CrossRef]

35. Seeliger, U.; Cordazzo, C.V.; Oliveira, C.P.L.; Seeliger, M. Long-Term Changes of Coastal Foredunes in the Southwest Atlantic. *J. Coast. Res.* **2000**, *4*, 1068–1072.

36. Villwock, J.A. Geology of the Coastal Province of Rio Grande Do Sul. *Pesquisas* **1984**, *16*, 5–49.

37. Villwock, J.A.; Tomazelli, L.J.; Loss, E.L.; Dehnhardt, E.A.; Bachi, F.A.; Dehnhardt, B.A. Geology of the Rio Grande Do Sul Coastal Province. In *Quaternary of South America and Antarctic Peninsula*; CRC Press: Boca Raton, FL, USA, 1986; Volume 4, pp. 79–97.

38. Villwock, J.A.; Tomazelli, L.J. Geologia Costeira Do Rio Grande Do Sul. *Notas Técnicas* **1995**, *8*, 1–45.

39. Tomazelli, L.J.; Villwock, J.A. Considerações Sobre o Ambiente Praial e a Deriva Litorânea de Sedimentos Ao Longo Do Litoral Norte Do Rio Grande Do Sul. *Pesquisas* **1992**, *19*, 3–12. [CrossRef]

40. Hesp, P.A.; Dillenburg, S.R.; Barboza, E.G.; Tomazelli, L.J.; Ayup-Zouain, R.N.; Esteves, L.S.; Gruber, N.L.S.; Toldo, E.E.; Tabajara, L.L.C.D.A.; Clerot, L.C.P. Beach Ridges, Foredunes or Transgressive Dunefields? Definitions and an Examination of the Torres to Tramandaí Barrier System, Southern Brazil. *An. Acad. Bras. Cienc.* **2005**, *77*, 493–508. [CrossRef]

41. Hesp, P.A.; Thom, B.G. Geomophology and Evolution of Active Transgressive Dunefields. In *Coastal Dunes: Form and Process*; Nordstrom, K.F., Psuty, N.P., Carter, R.W.G., Eds.; Jonh Wiley & Sons Ltd: Hoboken, NJ, USA, 1990; pp. 253–288.

42. Bigarella, J.J.; Klein, A.H.D.; Menezes, J.T.; Vintem, G. Southern Brazilian Coastal Dunes: Movement and Structures. *J. Coast. Res.* **2006**, *39*, 1–15.

43. Tomazelli, L.J. Contribuição Ao Estudo Dos Sistemas Deposicionais Holocênicos Do Nordeste Da Província Costeira Do Rio Grande Do Sul, Com Ênfase No Sistema Eólico. Tese de Doutorado, Universidade Federal do Rio Grande do Sul, Porto Alegre, Brasil, 1990.

44. Giannini, P.C.F. Sistemas Deposicionais Do Quaternário Costeiro Entre Jaguaruna e Imbituba, SC. Ph.D. Thesis, Universidade Estadual de São Paulo: São Paulo, Brazil, 1993.

45. Tomazelli, L.J.; Barboza, E.G.; Rosa, L.M.C.C. Geomorfologia e Potencial de Preservação Dos Campos de Dunas Transgressivos de Cidreira e Itapeva, Litoral Norte Do Rio Grande Do Sul, Brasil. *Pesquisas Geociências* **2008**, *35*, 47–55. [CrossRef]

46. Esteves, L.S. Variabilidade Espacio-Temporal Dos Deslocamentos Da Linha de Costa No Rio Grande Do Sul. Tese de Doutorado, Universidade Federal do Rio Grande do Sul, Porto Alegre, Brasil, 2004.

47. Portz, L.C.; Manzolli, R.P.; Gruber, N.L.S.; Correa, I.C.S. Turismo e Degradação Na Orla Do Rio Grande Do Sul: Conflitos e Gerenciamento. *Desenvolv. E Meio Ambiente* **2010**, *22*, 153–166. [CrossRef]

48. Portz, L.; Manzolli, R.P.; Hermanns, L.; Alcántara Carrió, J. Evaluation of the Efficiency of Dune Reconstruction Techniques in Xangri-Lá (Rio Grande Do Sul, Brazil). *Ocean. Coast. Manag.* **2015**, *104*, 78–89. [CrossRef]

49. Portz, L.; Jardim, J.P.M.; Manzolli, R.P.; Gruber, N.S. Impacts on the Dunes System: Natural Dynamic versus Anthropogenic Interference. *Ambiente Sociedade* **2016**, *19*, 135–154. [CrossRef]

50. Portz, L.; Manzolli, R.P.; Alcántara-Carrió, J.; Rockett, G.C.; Barboza, E.G. Degradation of a Transgressive Coastal Dunefield by Pines Plantation and Strategies for Recuperation (Lagoa Do Peixe National Park, Southern Brazil). *Estuar. Coast. Shelf. Sci.* **2021**, *259*, 107483. [CrossRef]

51. MMA (Ministério do Meio Ambiente) Sitio Ransar. Parque Nacional Da Lagoa Do Peixe. Planejamento Para o Sucesso Da Conservação. Secretaria de Biodiversidade e Florestas. Gerência de Biodiversidade Aquática e Recursos Pesqueiros. Available online: http://www.mma.gov.br/publicacoes/biodiversidade/category/53-biodiversidade-aquatica.html (accessed on 5 November 2019).

52. Moraes, V.L. Uso Do Solo e Conservação Ambiental No Parque Nacional Da Lagoa Do Peixe e Entorno (RS). Master's Dissertation, Universidade Federal do Rio Grande do Sul, Porto Alegre, Brasil, 2009; p. 120.

53. Martinho, C.T.; Dillenburg, S.R.; Hesp, P. Wave Energy and Longshore Sediment Transport Gradients Controlling Barrier Evolution in Rio Grande Do Sul, Brazil. *J. Coast. Res.* **2009**, *252*, 285–293. [CrossRef]

54. Camargo, O.A.; Silva, F.J.L. *Atlas Eólico: Rio Grande Do Sul*; SEMC-Secretaria de Energia Minas e Comunicações: Porto Alegre, Brazil, 2002.

55. NIMER, E. *Climatologia Do Brasil*; IBGE: Rio de Janeiro, Brazil, 1989.

56. Martinho, C.T. Morfodinâmica e Evolução de Campos de Dunas Transgressivos Quaternários Do Litoral Do Rio Grande Do Sul. Doctorate Dissertation, Universidade Federal do Rio Grande do Sul: Porto Alegre, Brasil, 2008; p. 215.

57. da Motta, L.M.; Toldo, E.E.; de Sá, L.E.; de Almeida, B.; Nunes, J.C. Sandy Sediment Budget of the Midcoast of Rio Grande Do Sul, Brazil. *J. Mar. Res.* **2015**, *73*, 49–69. [CrossRef]

58. Martinho, C.T.; Dillenburg, S.R.; Hesp, P.A. Mid to Late Holocene Evolution of Transgressive Dunefields from Rio Grande Do Sul Coast, Southern Brazil. *Mar. Geol.* **2008**, *256*, 49–64. [CrossRef]

59. Bitencourt, V.J.B.; Dillenburg, S.R.; Manzolli, R.P.; Barboza, E.G. Control Factors in the Evolution of Holocene Coastal Barriers in Southern Brazil. *Geomorphology* **2020**, *360*, 107180. [CrossRef]

60. Bitencourt, V.J.B.; Dillenburg, S.R.; Barboza, E.G.; Rosa, M.L.C.D.C.; Manzolli, R.P. Padrões De Empilhamento Estratigráfico E Seus Reflexos Na Morfologia Da Barreira Costeira Holocênica No Litoral Médio Do Rio Grande Do Sul, Brasil. *Rev. Bras. De Geomorfol.* **2020**, *21*, 529–548. [CrossRef]

61. Bitencourt, V.J.B.; Dillenburg, S.R. Application of Multivariate Statistical Techniques in Alongshore Differentiation of Coastal Barriers. *Mar. Geol.* **2020**, *419*, 106077. [CrossRef]

62. Toldo, E.E., Jr.; Almeida, L.E.S.B.; Nicolodi, J.L.; Absalonsen, L.; Gruber, N.L.S. O Controle Da Deriva Litorânea No Desenvolvimento Do Campo de Dunas e Da Antepraia No Litoral Médio Do Rio Grande Do Sul. *Pesqui. Em Geociências* **2006**, *33*, 35–42. [CrossRef]

63. Dillenburg, S.R.; Barboza, E.G.; Tomazelli, L.J.; Hesp, P.A.; Clerot, L.C.P.; Ayup-Zouain, R.N. The Holocene Coastal Barriers of Rio Grande Do Sul. In *Geology and Geomorphology of Holocene Coastal Barriers of Brazil*; Dillenburg, S.R., Hesp, P.A., Eds.; Springer: Berlin/Heidelberg, Germany, 2009; pp. 53–91.

64. Fryberger, S.G.; Dean, G. Dune Forms and Wind Regime. In *A Study of Global Sand Seas*; McKee, E.D., Ed.; US Geological Survey Professional Paper: Washington, DC, USA, 1979; pp. 137–169.

65. Bagnold, R.A. *The Physics of Blown Sand and Desert Dunes*; Methuen: London, UK, 1941.

66. Alcántara-Carrió, J.; Alonso, I. Measurement and Prediction of Aeolian Sediment Transport at Jandía Isthmus (Fuerteventura, Canary Islands). *J. Coast. Res.* **2002**, *18*, 300–315.

67. Revollo Sarmiento, G.; Cipolletti, M.; Perillo, M.; Delrieux, C.; Perillo, G. Methodology for Classification of Geographical Features with Remote Sensing Images: Application to Tidal Flats. *Geomorphology* **2015**, *257*, 10–22. [CrossRef]

68. Portz, L.; Rockett, G.C.; Franchini, R.A.L.; Manzolli, R.P.; Gruber, N.L.S. Gestão de Dunas Costeiras: O Uso de Sistema de Informações Geográficas (SIG) Na Implantação de Planos de Gestão No Litoral Do Rio Grande Do Sul, Brasil. *Rev. Gestão Costeira Integr.* **2014**, *14*, 517–534. [CrossRef]

69. Ludwig, A.; Meyer, H.; Nauss, T. Automatic Classification of Google Earth Images for a Larger Scale Monitoring of Bush Encroachment in South Africa. *Int. J. Appl. Earth Obs. Geoinf.* **2016**, *50*, 89–94. [CrossRef]

70. Lorenz, R.D.; Gasmi, N.; Radebaugh, J.; Barnes, J.W.; Ori, G.G. Dunes on Planet Tatooine: Observation of Barchan Migration at the Star Wars Film Set in Tunisia. *Geomorphology* **2013**, *201*, 264–271. [CrossRef]

71. Lipp-Nissinen, K.H.; Piñeiro, B.D.S.; Miranda, L.S.; Alves, A.d.P. Temporal Dynamics of Land Use and Cover in Paurá Lagoon Region, Middle Coast of Rio Grande Do Sul (RS), Brazil. *Rev. Gestão Costeira Integr.* **2018**, *18*, 25–39. [CrossRef]

72. Liang, J.; Gong, J.; Li, W. Applications and Impacts of Google Earth: A Decadal Review (2006–2016). *ISPRS J. Photogramm. Remote Sens.* **2018**, *146*, 91–107. [CrossRef]

73. Hu, Q.; Wu, W.; Xia, T.; Yu, Q.; Yang, P.; Li, Z.; Song, Q. Exploring the Use of Google Earth Imagery and Object-Based Methods in Land Use/Cover Mapping. *Remote Sens.* **2013**, *5*, 6026–6042. [CrossRef]

74. Vaz, D.A.; Sarmento, P.T.K.; Barata, M.T.; Fenton, L.K.; Michaels, T.I. Object-Based Dune Analysis: Automated Dune Mapping and Pattern Characterization for Ganges Chasma and Gale Crater, Mars. *Geomorphology* **2015**, *250*, 128–139. [CrossRef]

75. Xia, J.; Dong, P. A GIS Add-in for Automated Measurement of Sand Dune Migration Using LiDAR-Derived Multitemporal and High-Resolution Digital Elevation Models. *Geosphere* **2016**, *12*, 1316–1322. [CrossRef]

76. Rubin, D.M. A Unifying Model for Planform Straightness of Ripples and Dunes in Air and Water. *Earth-Sci. Rev.* **2012**, *113*, 176–185. [CrossRef]

77. Zimbelman, J.R.; Scheidt, S.P. Precision Topography of a Reversing Sand Dune at Bruneau Dunes, Idaho, as an Analog for Transverse Aeolian Ridges on Mars. *Icarus* **2014**, *230*, 29–37. [CrossRef]

78. Jackson, D.W.T.; Cooper, A.; Green, A.; Beyers, M.; Guisado-Pintado, E.; Wiles, E.; Benallack, K.; Balme, M. Reversing Transverse Dunes: Modelling of Airflow Switching Using 3D Computational Fluid Dynamics. *Earth Planet. Sci. Lett.* **2020**, *544*, 116363. [CrossRef]

79. Cooper, J.A.G. Mesoscale Geomorphic Change on Low Energy Barrier Islands in Chesapeake Bay, U.S.A. *Geomorphology* **2013**, *199*, 82–94. [CrossRef]

80. Selby, M.J.; Rains, R.B.; Palmer, R.W.P. Eolian Deposits of the Ice-Free Victoria Valley, Southern Victoria Land, Antarctica. *N. Z. J. Geol. Geophys.* **1974**, *17*, 543–562. [CrossRef]

81. Burkinshaw, J.R.; Rust, I.C. Aeolian Dynamics on the Windward Slope of a Reversing Transverse Dune, Alexandria Coastal Dunefield, South Africa. In *Aeolian Sediments*; 1993; pp. 13–21; ISBN 9781444303971. Available online: https://onlinelibrary.wiley.com/doi/abs/10.1002/9781444303971.ch2 (accessed on 5 November 2019).

82. Rubin, D.M. Lateral Migration of Linear Dunes in the Strzelecki Desert, Australia. *Earth Surf. Process. Landf.* **1990**, *15*, 1–14. [CrossRef]

83. Marín, L.; Forman, S.L.; Valdez, A.; Bunch, F. Twentieth Century Dune Migration at the Great Sand Dunes National Park and Preserve, Colorado, Relation to Drought Variability. *Geomorphology* **2005**, *70*, 163–183. [CrossRef]

84. Rockett, G.C.; Hesp, P.; Portz, L.; Barboza, E.G. Aeolian Geodiversity of the Itapeva Dunefield (Brazil) and Geoconservation in the Management of Protected Areas. *Geoheritage* **2022**, *14*, 111. [CrossRef]

85. Parise, C.K.; Calliari, L.J.; Krusche, N. Extreme storm surges in the south of brazil: Atmospheric conditions and shore erosion. *Braz. J. Oceanogr.* **2009**, *57*, 175–188. [CrossRef]

86. Machado, A.A.; Calliari, L.J. Synoptic Systems Generators of Extreme Wind in Southern Brazil: Atmospheric Conditions and Consequences in the Coastal Zone. *J. Coast. Res.* **2016**, *75*, 1182–1186. [CrossRef]

87. Martínez, M.L.; Landgrave, R.; Silva, R.; Hesp, P. Shoreline Dynamics and Coastal Dune Stabilization in Response to Changes in Infrastructure and Climate. *J. Coast. Res.* **2019**, *92*, 6. [CrossRef]

88. Levin, N.; Kidron, G.J.; Ben-Dor, E. The Spatial and Temporal Variability of Sand Erosion across a Stabilizing Coastal Dune Field. *Sedimentology* **2006**, *53*, 697–715. [CrossRef]

89. Costas, S.; Gallego-Fernández, J.B.; Bon de Sousa, L.; Kombiadou, K. Ecogeomorphic Response of a Coastal Dune in Southern Portugal Regulated by Extrinsic Factors. *Catena* **2023**, *221*, 106796. [CrossRef]

90. Lopez, A.C.B.; Hesp, P.A. Evolution of a Coastal Transgressive Dunefield to a Parabolic Dunefield, Canunda Dunes, South Australia. *Geomorphology* **2023**, *430*, 108653. [CrossRef]

91. Hesp, P.A. Conceptual Models of the Evolution of Transgressive Dune Field Systems. *Geomorphology* **2013**, *199*, 138–149. [CrossRef]
92. Tsoar, H. Sand Dunes Mobility and Stability in Relation to Climate. *Phys. A Stat. Mech. Its Appl.* **2005**, *357*, 50–56. [CrossRef]
93. Belly, P.Y. *Sand Movement by Wind*; Washington, DC, USA, 1964. Available online: https://repository.tudelft.nl/islandora/object/uuid:f5051163-7a83-440d-9d02-92683a442549/datastream/OBJ/download (accessed on 5 November 2019).
94. Sherman, D.J. Evaluation of Aeolian Sand Transport Equations Using Intertidal-Zone Measurements, Saunton Sands, England. *Sedimentology* **1990**, *37*, 385–392. [CrossRef]
95. Logie, M. Influence of Roughness Elements and Soil Moisture on the Resistance of Sand to Wind Erosion. Acidic soils and geomorphic processes. In Proceedings of the International Conference of the International Society of Soil Science, Jerusalem, Israel, 19 March–4 April 1981.
96. Sarre, R.D. Evaluation of Aeolian Sand Transport Equations Using Intertidal Zone Measurements, Saunton Sands, England. *Sedimentology* **1988**, *35*, 671–679. [CrossRef]
97. Guimarães, L.S. Morfodinâmica e Migração Das Dunas Eólicas Na Reserva Ecológica Do Taim, Litoral Sul Do RS. Master's Dissertation, Universidade Federal do Rio Grande do Sul, Porto Alegre, Brasil, 2005.
98. Puhl, P.R.; Dillenburg, S.R. Controls in the Development of Transgressive Dune Fields of the Holocene Coastal Barrier, Northern Coast of Rio Grande Do Sul. *Pesqui. Em Geocienc.* **2018**, *45*, 1–22. [CrossRef]
99. Rockett, G.C.; Telles, P.; Barboza, E.G.; Gruber, N.L.S.; Simão, C.E. Análise Espaço-Temporal Dos Ventos No Extremo Norte Da Planície Costeira Do Rio Grande Do Sul, Brasil. *Pesqui. Em Geocienc.* **2017**, *44*, 203–220. [CrossRef]